An investigation of the laser-induced zircon 'matrix effect'

E. Marillo-Sialer[1*], J. Woodhead[1], J.M. Hanchar[2], S.M. Reddy[3], A. Greig[1], J. Hergt[1], B. Kohn[1]

[1]School of Earth Sciences, The University of Melbourne, Parkville, Vic 3010, Australia

[2]Department of Earth Sciences, Memorial University of Newfoundland, St. John's, NL A1B 3X5, Canada

[3]The Institute for Geoscience Research, Department of Applied Geology, Curtin University, GPO Box U1987, Perth, WA 6845, Australia

*corresponding author: marillo@student.unimelb.edu.au

Abstract

This study aims to improve our understanding of the current limitations to high-precision U-Pb analysis of zircon by LA-ICP-MS by investigating the underlying causes of variation in ablation behaviour between different zircon matrices. Multiple factors such as: the degree of accumulated radiation damage; trace element composition; crystal colour; and crystallographic orientation are all systematically investigated. Due to the marked decrease in elastic moduli of natural zircon crystals with increasing radiation damage, the accumulation of this damage is the dominant factor controlling the rate of ablation for partially damaged to highly metamict zircon samples. There are slight differences, however, in ablation behaviour between highly crystalline matrices that cannot be attributed solely to differences in the degree of accumulated radiation damage. These differences are associated with structural weakening (i.e., decrease in elastic moduli and overall lower mechanical resistance) caused by an increasing degree of cation substitution in some of the zircon samples. Effects of crystallographic orientation and of crystal opacity (i.e., colour) on ablation behaviour are negligible compared to the combined influences of accumulated radiation damage and trace element substitution into the zircon structure. Experiments performed on natural and annealed zircon grains reveal that the reduction in ablation rates observed for the treated samples compared to the untreated grains is proportional to the degree of structural reconstitution achieved after annealing. Thermal annealing of natural zircon at temperatures > 1000 °C results in much more uniform ablation characteristics. This 'homogenisation' of ablation behaviour between zircon matrices produces a decrease in the laser-induced matrix effects and subsequent improvement in the accuracy of $^{206}Pb/^{238}U$ ratio determinations by LA-ICP-MS.

Keywords:

Laser ablation; zircon; matrix effects; U-Pb geochronology; annealing; Raman spectroscopy

1. Introduction

The uptake of laser ablation-inductively coupled plasma mass spectrometry (LA-ICP-MS) as an essential tool for rapid, cost-effective and high spatial resolution dating of zircon has been unprecedented (e.g., Schoene, 2014). Unfortunately, however, the matrix dependency of the ablation process remains a major drawback of the current method, limiting its accuracy and precision. Currently, LA-ICP-MS is routinely used to generate zircon U-Pb ages with an accuracy of ~2-3% (2σ) relative to the long-established benchmark thermal ionisation mass spectrometry (TIMS) U-Pb analysis of bulk zircon (e.g., individual grains or parts of grains; Schaltegger et al., 2015). The potential for any improvement in these figures appears to be influenced by systematic biases, which are associated with matrix differences between unknowns and the reference zircon materials used for standardization (e.g. Klötzli et al., 2009; Košler et al., 2013). These effects are further aggravated by the fact that it is unusual for ‘unknown’ natural zircon samples to share the traits that characterise a zircon reference material (i.e., well-ordered crystalline materials without many inclusions). It is now clear that the mitigation of these laser-induced ‘matrix effects’ will only be possible if the underlying causes are identified and understood.

Recent studies have linked the analytical bias between LA-ICP-MS dates and those determined by TIMS to the differential response of unknown and standard zircon materials to laser radiation (Marillo-Sialer et al., 2014; Steely et al., 2014). Although the underlying causes of this variable response have not yet been fully elucidated, a variety of factors are thought to influence the ablation efficiency (i.e., coupling of the laser to the material being ablated), such as crystal chemistry (Black et al., 2004), crystal colour (Kooijman et al., 2012), amount of accumulated radiation damage (Allen and Campbell, 2012; Steely et al., 2014) and crystal orientation (Mikova et al., 2009). The present study takes a systematic approach to investigating the relative importance of each of these factors.

In general, when using a single wavelength of pulsed laser light at constant laser fluence, differences in ablation rates arise from differences in absorptivity between samples (Horn et al., 2001). The absorption of radiation by accessory minerals, such as zircon, is strong in the ultraviolet (UV). For this reason, either excimer lasers operating at 193 nm (ArF) or solid state lasers operating at 213 nm (Nd:YAG) are now the norm for the analysis of these materials. However, slight changes in the degree of absorptivity between different zircon samples due, for example, to the presence of an increasing concentration of trace elements absorbing in the UV range of the laser, could lead to differences in the optical penetration depth of the laser beam and thus result in significant variations in rates of material removal. Horn et al. (2001) reported such variations in ablation behaviour among the NIST SRM 61X series glasses and correlated this with absorptivity of the sample, i.e., sample colour. This effect was noted when using a 266 nm Nd-YAG laser, but no apparent variation in ablation efficiency was observed when using a 193 nm excimer laser.

Structural damage produced by the process of alpha-decay also imparts a pronounced effect on the crystal structure and properties of natural zircon which could, in principle, alter the response to laser radiation. It is known that properties such as density, birefringence, hardness, compressibility and thermal conductivity, among others, change as a function of increasing radiation dose (Holland and Gottfried, 1955; Özkan, 1976; Chakoumakos et al., 1991; Oliver and McCallum, 1994; Ewing et al., 2003; Salje, 2006). Thus, for example, Steely et al. (2014) reported a close relationship between the degree of crystallinity of zircon samples and their laser penetration depth. However, an exclusive dependence of the ablation behaviour on the degree of structural distortion caused by alpha radiation could not be confirmed since the variations in ablation rates could also have been caused by other factors including the change in crystal colour, and thus be triggered by variations in the degree of optical absorption of the laser light. Furthermore, zircon shows different optical and mechanical properties on different crystallographic planes (Finch and Hanchar, 2003) that might also affect the rate at which the zircon ablates.

It is clear from the above that there are a multiplicity of factors potentially influencing the extent of laser coupling to the zircon target. It is therefore highly probable that the observed variability in ablation behaviour between zircon matrices is due to a combination of some or all the factors listed above and that no simple generalization is possible. This study represents a first attempt to systematically investigate the multiple variables affecting the rate of material removal as a function of the zircon properties. Our approach was designed to simplify the highly complex physical phenomena of laser-material interaction to a one-dimensional case. This was achieved by careful consideration of experimental design, as well as appropriate zircon sample selection, as detailed below.

2. Analytical approach, instrumentation and methods

Our study is composed of three parts. In the first part, the amount of accumulated radiation damage is used to evaluate the extent to which zircon matrices with different properties respond to laser radiation. In the second part, we investigate the role played by trace element composition on the different optical absorption properties of zircon crystals, and thus on their ablation behaviour. Finally, we evaluate the role that crystallographic orientation and crystal colour plays on the ablation behaviour.

2.1. Zircon samples and sample preparation

Several well-characterized zircon reference materials from various rock types were selected in order to study the relationship between crystal structure and ablation behaviour. These included the 02123 (295 ± 1 Ma, 2σ; Ketchum et al. 2001), 91500 ($^{206}Pb/^{238}U$ age 1062.4 ± 0.8 Ma, 2σ; Wiedenbeck et al. 1995), AS-3 ($^{206}Pb/^{238}U$ age 1099 ± 0.7 Ma, 2σ; Schmitz et al. 2003), FC-1 ($^{206}Pb/^{238}U$ age 1099.9 ± 1.1 Ma, 2σ; Paces and Miller 1993), Mt Dromedary ($^{206}Pb/^{238}U$ age 99.12 ± 0.02 Ma, 2σ; Schoene et al. 2006), Plešovice ($^{206}Pb/^{238}U$ age 337.13 ± 0.37 Ma, 2σ; Sláma et al. 2008), QGNG ($^{206}Pb/^{238}U$ age 1842 ± 3.1 Ma, 2σ; Black et al. 2003), Qinghu ($^{206}Pb/^{238}U$ age 159.38 ± 0.12 Ma, 2σ; Li et al. 2013), R-33 ($^{206}Pb/^{238}U$ age 419.26 ± 0.39 Ma, 2σ; Black et al. 2004), Seiland (531 ± 2 Ma, Pedersen et al., 1989), and Temora-2 ($^{206}Pb/^{238}U$ age 416.4 ± 0.4 Ma, 2σ; Black et al. 2004) zircons. These materials encompass a wide range of U-Pb ages, U and Th contents and thus, accumulated radiation damage. U and Th contents range from ~30 – 3000 $\mu g\ g^{-1}$ and ~20 – 1200 $\mu g\ g^{-1}$, respectively. Several grains of each zircon were mounted in epoxy-discs. The epoxy mounts were diamond polished and cleaned using standard techniques. Zircon grains were then examined by means of scanning electron microscope (SEM) and imaged with cathodoluminescence (CL). The images were used to identify inclusions and fractures within the zircon grains and to reveal internal zonation patterns and irregular domains. Additionally, optical inspection of the zircon samples was done by conventional reflected and transmitted microscopy.

In the second part of this study, we made use of synthetically grown zircon crystals thereby eliminating the accumulated radiation damage component. The synthetic samples include undoped, Hf-doped, Gd^{3+}-and P-doped, Dy^{3+}-and P-doped, Er^{3+}-and P-doped, Yb^{3+}-and P-doped, Y^{3+}-and P-doped zircon crystals, as well as zircon crystals doped with Gd^{3+}, Dy^{3+}, Er^{3+}, Yb^{3+}, Y^{3+}-and P at two different doping levels. Details regarding synthesis and the properties of these materials can be found in Finch et al. (2001), Hanchar and Finch (2001), Fisher et al. (2011). Using synthetic zircon crystals to evaluate the effects of chemical composition on the ablation behaviour of zircon has certain advantages over the use of natural zircon samples. These include the absence of U and Th in their structure, and therefore the lack of radiation-induced damage; the availability of crystals doped with individual rare-earth elements (REE) and Hf, and the high level of doping achievable. The latter may provide a means of augmenting any effect that the trace element composition may have on the ablation behaviour, thus making it more noticeable. As with their natural counterparts, the synthetic samples were mounted in a single epoxy disc, polished and cleaned using the standard procedures. It was ensured that the crystals were mounted with their *c*-axis parallel to the surface of the epoxy mount to avoid potential variations in the ablation behaviour arising from different crystallographic orientations.

For the third part of this study, we selected four relatively large (centimeter-size) zircon crystals derived from the Mud Tank carbonatite suite (U-Pb TIMS age of 731.65 ± 0.49 Ma; Horstwood et al., 2016). These were chosen due to their high degree of crystallinity, i.e., negligible structural damage, in order to avoid the ambiguity that may occur in the simultaneous analysis of two or more variables (e.g., radiation damage and crystal orientation) that could potentially affect the ablation behaviour. The selected crystals have well-developed faces and colours ranging from nearly colourless to brown (**Figure 1a**). The colour of each crystal has been visually estimated using the following colour and intensity coding: pale orange (MT0), orange (MT1), red (MT2) and brown (MT3). Preliminary crystal orientation was defined using the well-developed (100) or (010) faces of the zircon crystals. The crystals were cut parallel and perpendicular to the *c*-axis using a diamond saw as depicted in **Figure 1b**. The prepared sections were mounted in epoxy resin and their exact crystallographic orientation was then determined by electron backscatter diffraction (EBSD) as described below. The remaining section of each crystal was crushed and a few shards of < 3 mm length were separated, weighed and digested for solution ICP-MS analysis. Dissolution was achieved in high-pressure PTFE reaction vessels in an oven at 185 °C with HF-HNO_3 followed by HCl acids, and then finally taken up in HNO_3. An aliquot of each resultant solution was further diluted with a 1.8% HNO_3 solution containing an internal standard mixture (see below for details) to give a total dilution factor of 4000.

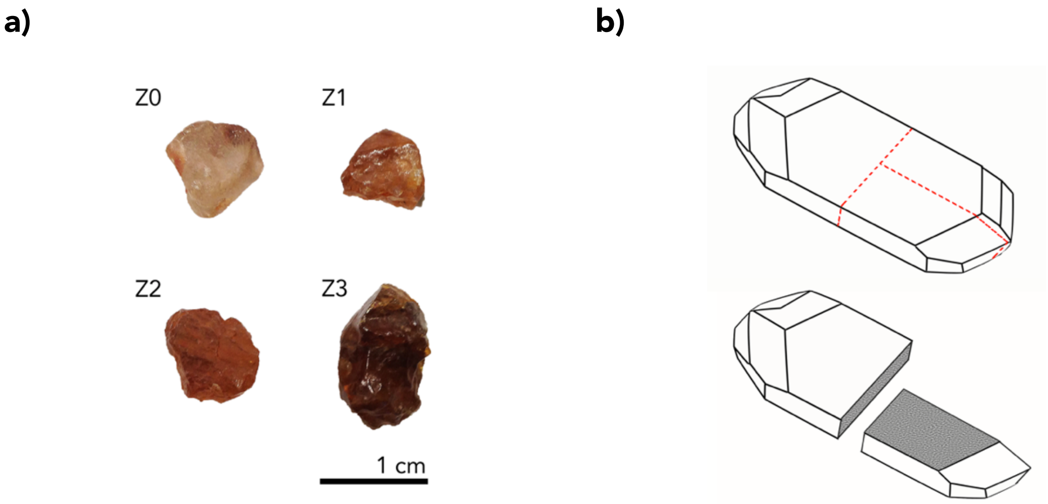

Figure 1 a) Mud Tank zircon crystals investigated in this study with colours ranging from pale orange (MT0), through orange (MT1) and red (MT2) to brown (MT3); b) Schematic representation of the crystal sectioning method for the investigation of crystallographic effects on ablation behaviour; (above) well-developed (100) or (010) crystal faces allowed the identification of the c-axis; (below) crystal sections produced after sectioning, grey areas show the crystal planes which were mounted parallel to the mount surface. The third crystal section was analysed for trace element content by ICP-MS.

2.2. Solution-ICP-MS analyses

The chemical composition of the Mud Tank zircon samples was determined by solution ICP-MS analysis on an Agilent 7700x instrument. Analytical procedures used are comprehensively described in Eggins et al. (1997). The method uses a natural rock reference material for calibration, internal drift correction using multi-internal standards (^{6}Li, ^{115}In, ^{185}Re, ^{209}Bi and ^{235}U), external drift monitors and aggressive washout procedures. Two minor modifications to the Eggins et al. (1997) protocol were made: 1) ^{84}Sr, ^{147}Sm, and ^{169}Tm, were not incorporated in the internal standard mixture; and 2) Two digestions of the USGS standard W-2 were used for instrument calibration. In addition, the preferred concentrations used for the W-2 reference material were derived by combining analyses of this material referenced to synthetic standards with a literature survey of appropriate isotope dilution analyses (**Table A1 in Appendix 1**; Kamber et al., 2003; Kamber et al., 2005; Babechuk et al., 2010).

The instrument was tuned to produce cerium oxide levels (CeO^+/Ce^+) of 1% or less and sensitivity better than 3.3×10^4 and 4.8×10^5 cps/ppb for ^{7}Li and ^{238}U, respectively. The uptake rate for the tune solution was 0.27 mL min$^-$

[1]. Four replicates of 100 scans per replicate were measured for each isotope. Dwell times ranged from 0.007−0.03 s depending on the analyte. The ^{152}Sm and ^{153}Eu isotopes were measured instead of the usual ^{147}Sm or ^{149}Sm and ^{151}Eu, respectively, in order to avoid or reduce ZrF_3 interferences. Long sample wash-out times of 6 minutes with solutions of 0.5% Triton X-100, 5% HNO_3, 0.025% HF in 5% HNO_3 and 2% HNO_3, and long sample uptake times of 120 seconds were used. A digestion of the GSJ basalt reference material JB-2 (Ando, 1984) was analysed as an unknown. Offline corrections were applied after data acquisition. ^{152}Sm was corrected for a minor ^{152}Gd isotope contribution and BaO^+ interferences. ^{153}Eu was corrected for ZrF_3 interference by analysing the levels in a Zr single-element solution. ^{153}Eu was also corrected for BaO^+ interference (i.e, $^{137}Ba^{16}O$).

2.3. Electron back scattered diffraction

Crystal orientations of the Mud Tank zircon sections embedded in epoxy resin were determined in order to investigate the effects of crystal orientation on ablation behaviour. The crystallographic orientation measurements were performed prior to LA-ICP-MS analysis. Prior to EBSD analysis the mount was polished with 0.06 μm colloidal silica to remove surface damage. EBSD analyses were undertaken on a Tescan MIRA3 Field Emission SEM, housed in the Microscopy & Microanalysis Facility (John de Laeter Centre) at Curtin University, Perth, Western Australia. Details of this system have recently been described elsewhere (Reddy et al., 2015). For each surface a 50x50 μm area was analysed by collecting diffraction patterns (**Figure A1 in Appendix 2**) at the nodes of a 1 μm (MT1, MT2, MT3) or 2 μm (MT0) spaced grid – a total of 8125 diffraction patterns. This area of analysis was undertaken to assess the potential presence of any small lattice orientations within the zircon grains. EBSD patterns were collected and indexed using Oxford Instruments Aztec 2 software. Indexing of empirically collected patterns was done using zircon match unit 5260 as recommended by Reddy et al. (2008). In all cases, indexing exceeded 95% with no systematic misindexing present in any of the zircon samples. Pole figures of zircon orientation, relative to a coordinate system fixed in the sample mount, were plotted to characterise the orientation of each zircon sample and analyse orientations within each analysed zircon grain (**Table A2 in Appendix 1**).

2.4. Raman spectroscopy

Radiation damage has a pronounced effect on the Raman spectrum of zircon. With increasing degree of structural disorder, the Raman bands of the zircon spectrum broaden and their frequencies shift towards lower wavenumbers. These effects are of considerable magnitude for the ν_3 stretching band of the (SiO_4) tetrahedral group (full width at half maximum - FWHM and wavenumber of synthetic zircon of 1.8 and ~1008 cm^{-1}, respectively; Nasdala et al., 2004). It has been previously demonstrated that the measured FWHM of the ν_3 (SiO_4) band is directly proportional to the amount of radiation damage accumulated in the zircon structure (Nasdala et al., 1995). For that reason, we have used Raman spectroscopy as an *in situ* method to quantitatively estimate the degree of crystallinity in the zircon grains in this study. Raman spectra were collected for several grains of the studied zircon samples in at least two spatially independent points before LA-ICP-MS analysis. Raman data were acquired focusing the 532 nm line of a frequency doubled Nd:YAG laser onto the polished surface of the zircon samples with a confocal microscope in a backscattering geometry. A Leica N Plan 50x objective lens with a numerical aperture of 0.75 resulted in a ~2 μm laser spot size with an output power of 15 mW and was used for all measurements. The diffraction-limited theoretical lateral and axial resolution at the sample surface are ~0.9 μm and 3.8 μm, respectively. Spectra were collected for 10 seconds with a Renishaw InVia Reflex 0.25 working distance micro-Raman spectrometer with a 2400 grooves/mm grating. The overall wavenumber error was estimated to be ±0.5 cm^{-1}. The spectral resolution was 1.1 cm^{-1} per CCD-pixel for a 2400 mm^{-1} grating. The Raman bands (shift at ~1000 cm^{-1}) were fitted assuming Voigt functions (Abrarov and Quine, 2011). Measured FWHM data were corrected for the linewidth broadening resulting from the spectrometer response following the approach described in Bergman et al. (1999) and references therein. The uncertainty in the FWHM is estimated to be better than ±0.4 cm^{-1} for FWHM < 20 cm^{-1} to ±1.5 cm^{-1} for FWHM ~25 cm^{-1}.

2.5. LA-ICP-MS

After characterization by Raman spectroscopy, the natural zircon samples were analysed by LA-ICP-MS for *in situ* U-Pb dating and trace element composition. A Resonetics RESOlution laser ablation system incorporating a two-volume ablation cell (Laurin Technic Pty) and a CompexPro 102 (Coherent, USA) 193 nm ArF excimer laser with a pulse width of 20 ns was used for analysis. The inner volume of the ablation chamber (~2 cm^3) is designed to provide a stratified atmosphere of He gas and He + Ar gas mixture, with ablation occurring in the lower He gas layer. The ablated material then rises due to plume expansion and is transported rapidly out of the ablation cell into the ICP-MS by the gas mixture (Eggins et al., 1998; Woodhead et al., 2004). All the experiments were done with constant He and Ar gas flows of 0.3 and ~1 L min^{-1}, respectively. Laser spot sizes of 20-40 µm were employed for different parts of this study. A laser repetition rate of 5 Hz and a laser fluence of ~2 J cm^{-2} were used in both sessions. Time-resolved trace element and U-Pb data were collected with an Agilent 7700x quadrupole ICP-MS. The acquisition parameters of the ICP-MS system were optimized before each analytical session to achieve high signal-to-noise ratio and low oxide production (ThO^+/Th^+ ratio of < 0.2%). The dwell time for each isotope was set at 10 ms for ^{29}Si, ^{31}P, ^{89}Y, ^{91}Zr, ^{140}Ce, ^{159}Tb, ^{163}Dy, ^{165}Ho, ^{166}Er, ^{169}Tm, ^{172}Yb, ^{175}Lu, ^{178}Hf and ^{208}Pb; 20 ms for ^{232}Th and ^{238}U; 30 ms for ^{206}Pb and 40 ms for ^{207}Pb. Gas background data were acquired for 20 s prior to each ~30 s spot ablation. A total of 16-21 single spot analyses of each zircon sample were done sequentially, with each zircon being alternated every two spot ablations, in order to monitor variations in ablation rate due to fluctuations in laser fluence within the analytical session. One analysis of the NIST 610 glass reference material was alternated every 8-10 measurements of the zircon samples. The 91500 zircon was used as primary reference material for all U-Pb age determinations. Trace element concentrations were calculated using NIST 610 as reference material and ^{29}Si as internal standard. Background subtraction and correction for laser induced fractionation (LIEF) of U-Pb ratio signals, as well as trace element content and weighted U-Pb age calculations, were performed using the Iolite software package (Paton et al., 2010; Paton et al., 2011).

2.6. Confocal laser scanning microscopy

The investigation of the resultant ablation pit depth is of particular interest in this study. We studied the post-ablation topography of the zircon samples using a confocal laser-scanning microscope (CLSM 700, Carl Zeiss). The CLSM uses optical sectioning to obtain high-resolution images of thin slices of the scanned area at different sample depths (i.e., along the *z*-axis) by removing the contribution of out-of-focus light in each image plane. The resulting images are then stacked in order to reconstruct a three-dimensional image of the ablation pit. The image planes were acquired using a 405 nm diode solid-state laser, a 50x magnification objective and 0.15-0.35 µm slice thickness. The ablation depth was obtained from the cross-section profile of the ablation pit by measuring the distance between the bottom of the ablation pit and the surface of the sample. The precision of the depth determinations was <1% (2σ), as estimated by repeatedly measuring the depth of a well-defined ablation pit. Ablation rates were calculated as the ratio between ablation depth and number of laser pulses used.

3. Results

3.1. Part I: Accumulated radiation damage

Figure 2 shows examples of Raman spectra obtained for the zircon samples investigated in this study. Two spectra are shown for each zircon sample, which correspond to the minimum (solid line) and maximum (dashed line) FWHM values measured for the ν_3 (SiO_4) band of spectra acquired at different spatial locations. It can be seen that the Mud Tank and 91500 zircons have highly crystalline structures, with ν_3 (SiO_4) FWHM and frequency close to those obtained for synthetic zircon: 1.8 cm^{-1} and 1008 cm^{-1}, respectively (Nasdala et al., 2004). In addition, average ν_3 (SiO_4) FWHMs were 2.5 ± 0.01 cm^{-1} for Mud Tank and 4.0 ± 0.07 cm^{-1} for 91500, indicating a very homogeneous distribution of accumulated radiation damage across their structure. The overall degree of crystallinity and homogeneity is slightly lower for the Mt Dromedary and Temora zircons, 4.8 ± 0.3 cm^{-1} and 4.5 ± 0.3 cm^{-1} respectively, which can be attributed to higher U and Th abundances and greater compositional zonation revealed by CL imaging. The Qinghu and Plešovice zircons show FWHM values for the ν_3 (SiO_4) band that correspond to moderately damaged zircon (~5 – 16 cm^{-1}), whereas QGNG and AS-3 zircons show highly variable FWHM, with values ranging from 9 – 28 cm^{-1}, characteristic of moderate to highly metamict zircon matrices (Nasdala et al., 1995). It should be noted that the Raman spectrum obtained for some AS-3 zircon grains showed no discernible peak between 900 cm^{-1} and 1100 cm^{-1}, but a broad spectral feature which is associated with the predominant occurrence of an amorphous phase in metamict zircon (Zhang et al., 2000b).

As mentioned above, radiation damage also has an effect on the frequency of the ν_3 (SiO_4) band in the Raman spectrum of zircon. Typically, measured ν_3 (SiO_4) wavenumbers follow a negative linear relation when plotted against corresponding FWHM values. It has been shown, however, that deviations from this trend occur (Geisler et al., 2001; Geisler and Pidgeon, 2002; Nasdala et al., 2002a) and that they are associated with structural modifications caused by incomplete recovery of the zircon structure due to heat-treatment or, in some cases, natural annealing. It follows that the relationship between FWHM and Raman shift in ν_3 (SiO_4) band position measured for our zircon samples, illustrated in **Figure 3**, provides a means of identifying zircon matrices that have undergone a post-magmatic thermal event and/or thermal treatment, and thus have not accumulated radiation damage completely. Our data show a linear correlation for FWHM ≤ 20 cm^{-1}. A slight change in slope occurs at FWHM ~20 cm^{-1}, i.e., for highly damaged zircon. A similar departure from linearity has been observed previously (Zhang et al., 2000b; Geisler et al., 2001; Geisler and Pidgeon, 2002; Nasdala et al., 2002a). Moreover, it can be seen that several data points of the QGNG sample lie above the trend line. This could be an indication that the QGNG zircon underwent partial recrystallization and chemical alteration associated with a natural annealing event (Geisler et al., 2001; Geisler and Pidgeon, 2002; Nasdala et al., 2002a; Geisler et al., 2003a).

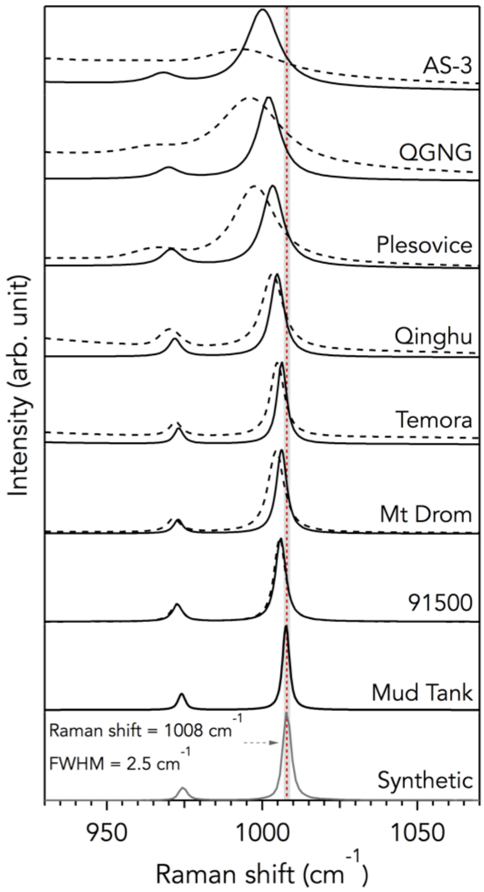

Figure 2 Examples of Raman spectra (900 - 1100 cm^{-1}) obtained in this study. The spectra were collected from zircon areas targeted for LA-ICP-MS analysis. Band broadening occurs as a result of increasing amount of accumulated radiation damage. Two spectra are shown for each natural zircon sample that represent the minimum (solid) and maximum (dashed) bandwidth of the $\nu_3 (SiO_4)$ Raman band measured for the corresponding sample. The difference between the two bands reveals the variation in degree of radiation damage across each natural zircon. The Raman spectrum of a synthetic undoped zircon is shown (bottom) for comparison ($\nu_3 (SiO_4)$ band frequency of 1008 cm^{-1}, dashed red line).

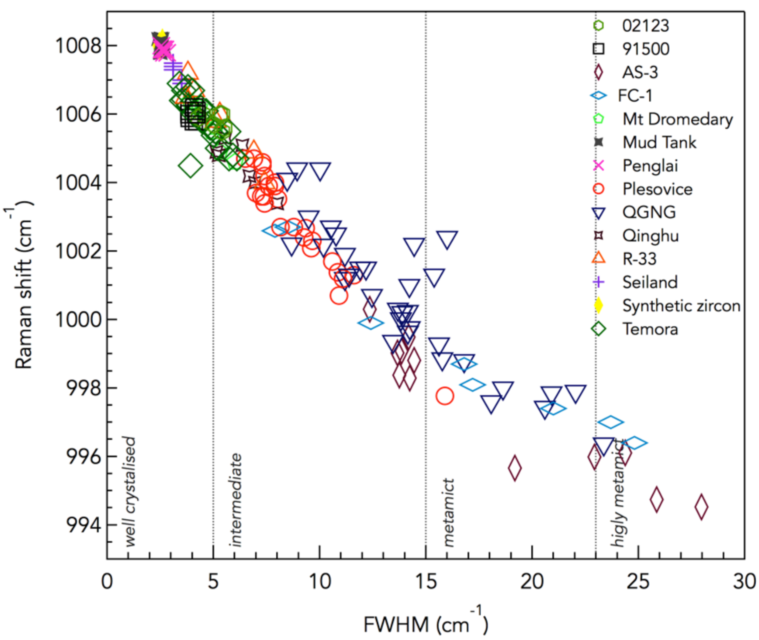

Figure 3 Raman shift (frequency) as a function of the FWHM of the $\nu_3 (SiO_4)$ band for all the spectra obtained in this study. Plotted data follow an almost linear trend. Note the slight deviation from linearity that occurs at FWHMs of ~20 cm^{-1}, which is attributed to the increasing volume fraction of the amorphous phase within the zircon structure. Zircon samples have been classified according to their degree of accumulated radiation damage (i.e., FWHM) as well-crystallised, intermediate, metamict and highly metamict (following Nasdala et al., 1995).

Figure 4 shows the correlation between FWHM values and zircon ablation rates (expressed as ablation rate offset, $\Delta AR_{(Smp-RM)}$). The drill rate offset values have been calculated relative to the average ablation rate obtained for the Temora zircon using the following equation:

$$\Delta AR_{(Smp-RM)}\% = \frac{AR_{Smp} - AR_{RM}}{AR_{RM}} \times 10^2 \qquad (1)$$

where AR_{RM} is the ablation rate of the zircon used for calibration (here the Temora zircon) and AR_{Smp} the ablation rate for the zircon sample. The fewer number of data points in **Figure 4**, compared to **Figure 3**, results from difficulties in characterising the dimensions (e.g., depth) of pits containing ablation artifacts resulting from surface irregularities such as microcracks, as described in detail in Evans et al. (2015). Since no peak was observed on the Raman spectra of the amorphous AS-3 zircon, values of FWHM ≥ 30 cm^{-1} (solid black diamonds) were assigned based on the intensity of the signal from the amorphous phase. These values are provided as a visual guide only. It can be seen in **Figure 4**, that an increase in bandwidth of the ν_3 (SiO_4) band in the Raman spectra of zircon (i.e., FWHM), and thus an increase in the degree of accumulated radiation damage, results in an apparent increase in ablation rates. However, given the scatter of the data about a straight line, there is a suggestion that there may be additional factors contributing to the observed differences in ablation efficiency, especially for the most crystalline zircon samples (ν_3 (SiO_4) FWHM ≤ 6 cm^{-1}) for which the scatter in measured ablation rates is rather significant considering the small differences in their degree of accumulated radiation damage.

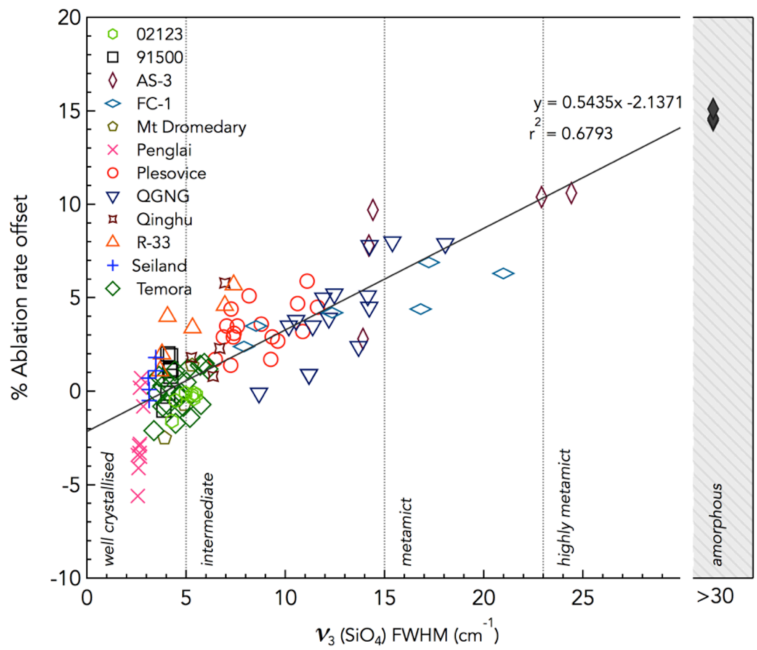

Figure 4 Ablation rate offset percent ($\Delta AR_{(Smp-RM)}$) as a function of the degree of radiation damage (FWHM). The individual drill rate offset values have been calculated relative to the average ablation rate value obtained for the Temora zircon. Values of FWHM ≥ 30 cm^{-1} (solid black diamonds) have been assigned to spectra of the AS-3 zircon where no discernible ν_3 (SiO_4) band was observed and they serve as a visual guide only. Linear regression of data pairs with FWHMs < 30 cm^{-1} are shown as a solid black line (n = 104, r^2 = 0.68). Note the considerable range in variability in ablation rates obtained for these zircon reference materials (i.e., ~16%).

3.1.1. The effect of thermal annealing on the ablation behaviour of zircon

An alternative approach to study the role of radiation-induced structural damage on the ablation behaviour of zircon is to evaluate the effect that damage removal by thermal annealing has on the ablation characteristics. The use of thermal annealing as sample pre-treatment for U-Pb zircon geochronology by LA-ICP-MS has been reported to be successful in improving the precision and accuracy of the technique (Allen and Campbell, 2012; Solari et al., 2015). However, contrasting cases where thermal-annealing has not been found advantageous in improving the accuracy have also been reported (Marillo-Sialer et al., 2014). It is clear that a more thorough analysis of the effects of annealing on our zircon reference materials is required to explain the contradictory nature of past observations and the potential for future applications. In this regard, the use of Raman spectrometry is particularly important because it enables quantitative determination of the degree of structural reconstitution (i.e., the level of defect recovery and short-range order) caused by thermal annealing.

As part of this study we used Raman spectroscopy to identify the structural changes that occurred in several zircon matrices after thermal treatment at two different temperatures for different heating times. Several grains of the Penglai, Plešovice, QGNG and Temora zircons were treated at 850 °C for 48 h. Annealing at these conditions led to discolouration of the zircon samples. The Penglai and Temora grains became colourless to the naked eye, whereas grains of the Plešovice and QGNG zircons turned bright orange. The treated zircon grains were mounted in an epoxy disc together with untreated examples of the same zircon matrices, and subsequently polished and cleaned as described earlier. Raman spectra were collected from multiple grains of each specimen. **Figure A2 in Appendix 2** shows examples of the spectra obtained for each zircon both before and after thermal treatment. In the Raman spectra of the untreated and treated Penglai zircon, the frequency and FWHM values of the ν_3 (SiO_4) band are very close to those obtained for the Mud Tank zircon, which correspond to a very well crystallised structure. In the case of the Temora, Plešovice and QGNG zircons, a subtle shift in position of the ν_3 (SiO_4) band towards higher frequencies can be observed after annealing. However, the width of the ν_3 (SiO_4) band in the Raman spectra of the annealed Plešovice and QGNG zircons seems to remain close to the peak width values obtained for those zircon materials before thermal treatment. These effects are more clearly seen in **Figure 5**. This more pronounced shift in Raman frequency relative to the decrease in bandwidth of the ν_3 (SiO_4) band has been previously observed for thermally treated zircon (Geisler et al., 2001, Nasdala et al., 2002a, and Nasdala et al., 2002b) and relates to partial structural recovery of moderately to highly metamict zircon grains annealed at temperatures < 900 °C. Note again that the Raman ν_3 (SiO_4) band in the spectra of Plešovice and QGNG zircons have FWHM values that are > 5 cm^{-1} indicating that there is still a significant portion of distorted SiO_4 tetrahedra present in their structure. For further reading on the effects of annealing on the structure of metamict zircon, the reader is referred to Geisler (2002).

As reported by Nasdala et al. (2002b), a dramatic increase of the crystalline fraction in moderate to highly metamict zircon matrices occurs only after annealing at temperatures > 950 °C. For that reason, it became evident that further information on the effects of annealing at temperatures other than 850 °C should be obtained in order to facilitate the assessment of the effects of thermal treatment on the ablation behaviour of zircon. We annealed multiple grains of the 02123, 91500, FC-1, Plešovice, R-33, Seiland and Temora zircon reference materials at 1000 °C for 36 h. As described above for zircon samples annealed at 850 °C, with the exception of Plešovice that turned bright orange, all the zircon matrices treated at 1000 °C lost their coloration and became translucent. Similarly, the treated zircon grains were mounted in an epoxy disc along with untreated specimens, and prepared correspondingly for Raman spectroscopy and LA-ICP-MS analyses. **Figure A3 in Appendix 2** shows a comparison of Raman spectra obtained between treated and untreated zircon samples. It can be observed that there has been a significant increase in frequency and decrease in bandwidth of the ν_3 (SiO_4) band in the Raman spectra of all the zircon materials treated at 1000 °C, with FWHM values similar to those obtained for well-crystallised zircon specimens, i.e., FWHM < 5 cm^{-1}. Raman data are shown in **Figure 6**, where it can be seen more clearly that annealing at 1000 °C caused a significant structural recovery in all the treated zircon samples (moderate to highly metamict).

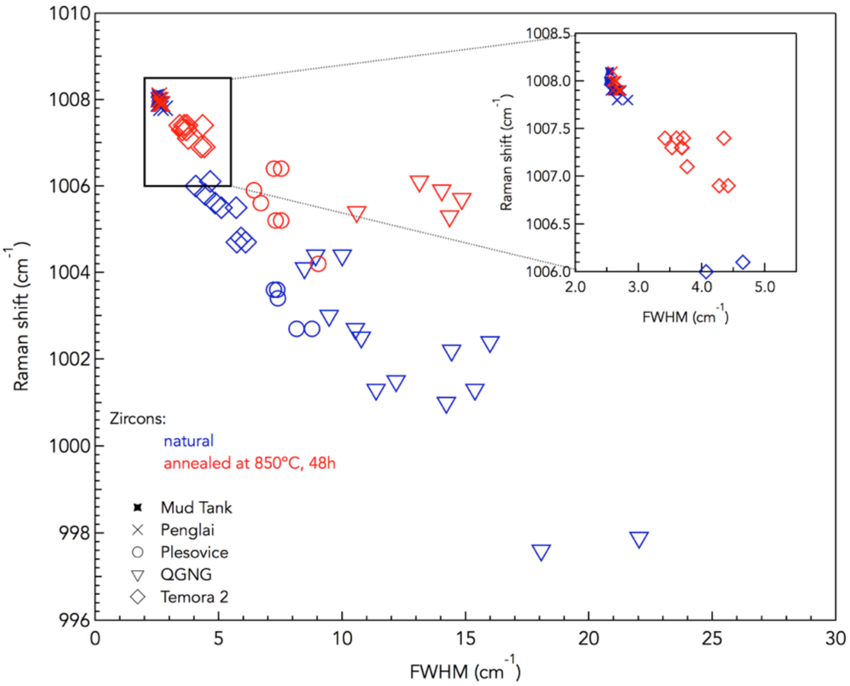

Figure 5 Raman shift (frequency, in cm^{-1}) versus FWHM values (bandwidth, cm^{-1}) corresponding to the anti-symmetric stretching vibration (ν_3) of SiO_4. Data were obtained for untreated (blue) and annealed at 850 °C for 48 h (red) Penglai, Plešovice, Temora and QGNG zircons. Data pairs of a well-crystallised, untreated zircon, i.e., Mud Tank, are shown for comparison.

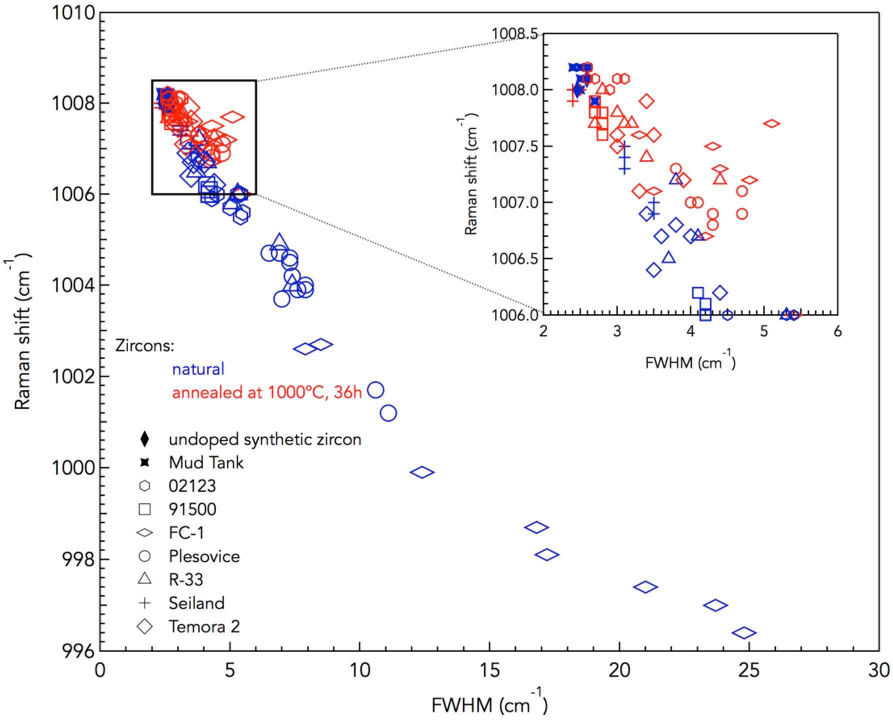

Figure 6 Raman shift (frequency, in cm^{-1}) versus FWHM values (bandwidth, cm^{-1}) corresponding to the anti-symmetric stretching vibration (ν_3) of SiO_4. Data were obtained for untreated (blue) and annealed at 1000 °C for 36 h (red) 02123, 91500, FC-1, Plešovice, R-33, Seiland and Temora zircons. Data pairs of a synthetic zircon sample, and of a well-crystallised, untreated zircon, i.e., Mud Tank, are shown for comparison.

Marillo-Sialer et al. (2014) studied the ablation behaviour of Temora, Plešovice and QGNG zircons annealed at 850 °C for 48 h. They found that annealing at those conditions has an effect on the ablation behaviour of zircon, in that it reduces the rate of ablation during (193 nm excimer) pulsed laser interaction. However, even after annealing the different zircon matrices still ablated at different rates, which affected the U/Pb ratios determined by LA-ICP-MS. The reduction in ablation rates observed for the annealed samples in Marillo-Sialer et al. (2014) might be closely associated with the partial recovery of the crystal structure as revealed by Raman spectrometry (**Figure 5**). Moreover, the variation in ablation rates observed between annealed samples can be explained by the remaining differences in the degree of structural damage, which are probably still too significant to allow homogenisation of the ablation behaviour between zircon matrices.

Given the moderate linear correlation between accumulated radiation damage and ablation rate observed in **Figure 4** and the reduction in ablation rate associated with annealing at 850 °C, it seems probable that moderate to highly metamict zircon treated at 1000 °C would behave similarly regarding their ablation characteristics. Therefore, in an attempt to further elucidate the effects of annealing at 1000 °C, we measured the ablation rates of pits produced by firing 175 laser pulses at a laser fluence of ~2.5 J cm^{-2}. The results are plotted in **Figure 7** in combination with ablation rates measured for untreated examples of the same zircon samples. It can be seen that annealing of zircon at 1000 °C for 36 h caused an overall reduction in the rate of ablation of treated samples relative to those of the untreated samples, as seen earlier for zircon matrices annealed at 850 °C (Marillo-Sialer et al., 2014). Moreover, the average ablation rates measured for the treated 02123, FC-1, R-33, Seiland and Temora zircons are similar to within uncertainty of the individual ablation depth determinations. In contrast, the treated Plešovice and 91500 zircons show ablation rates that are higher and lower, respectively, compared to those of the other annealed zircon samples.

We evaluated the effect that the modified ablation behaviour between most of the annealed zircon materials has on their measured LA-ICP-MS $^{206}Pb/^{238}U$ ages. **Figure 8** shows the relationship between $^{206}Pb/^{238}U$ age bias (relative to their accepted TIMS ages, $\Delta^{206}Pb/^{238}U\ Age$) and ablation rate offset values (relative to the untreated 91500 zircon, $\Delta AR_{(Smp-RM)}$). It is clear from the $^{206}Pb/^{238}U$ ages obtained on the annealed samples that the reduction in ablation rate offset led to an overall decrease in the age-offset scatter. We note, however, that there is still a discrepancy between ablation rates for the treated Plešovice zircon relative to the other annealed matrices, which accounts for the higher age offset observed for that sample. The higher ablation rates measured for the annealed Plešovice grains agree with the residual structural damage quantified by Raman spectroscopy for this sample compared to the other treated zircon matrices (**Figure 6**). Surprisingly, the FC-1 zircon, which likewise shows incomplete recovery of its crystal structure after annealing seems to ablate at rates similar to the other more crystalline zircon materials.

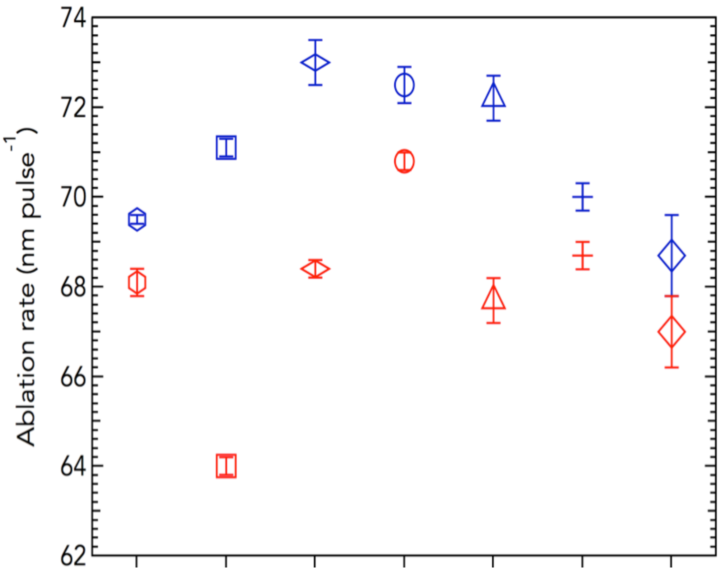

Figure 7 Ablation rates measured for untreated (blue) and annealed (1000 °C for 36 h; red) zircon samples. All the pits were ablated by firing 175 laser pulses at a laser fluence of ~2.5 J cm^{-2} during the same analytical session and under identical operating conditions. There is an overall reduction of the ablation rates for the annealed zircon samples compared to those of the untreated samples. The annealed 02123, FC-1, R-33, Seiland and Temora zircons show similar ablation behaviour, with ablation rate values that overlap within error of the pit depth determinations.

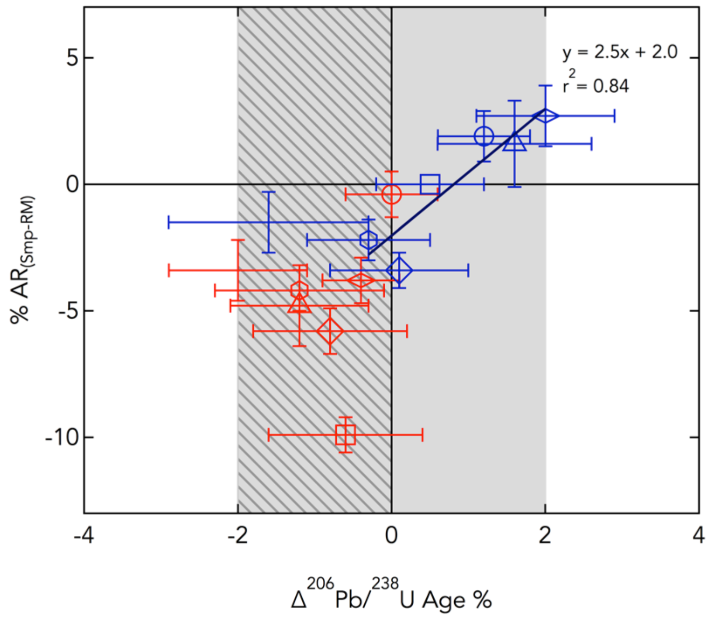

Figure 8 Ablation rate percent offset (*$\Delta AR_{(Smp\text{–}RM)}$) versus* ^{206}Pb/^{238}U age percent offset (*$\Delta^{206}Pb/^{238}U$ Age*) from the accepted TIMS age. Data from untreated (blue) and annealed at 1000 °C (red) zircon materials: (⬡) 02123, (□) 91500, (<>) FC-1, (○) Plešovice, (△) R-33, (+) Seiland and (◇) Temora. Ablation rate offsets were calculated relative to the ablation rate of the untreated 91500 zircon reference material (blue box). The regression line shows the linear correlation between ablation rate and ^{206}Pb/^{238}U age offsets observed for natural untreated zircon samples. The gray shaded area represents ±2% ^{206}Pb/^{238}U age uncertainty. Note the reduction in dispersion in ^{206}Pb/^{238}U age offset after thermal treatment (diagonal lines).

3.2. Part II: Chemical composition

In this part of the study we evaluated the ablation behaviour of various synthetic zircon crystals. The synthetic samples included pure zircon crystals (undoped), Hf-doped zircon crystals, as well as crystals doped with one or more REE^{3+}. The aim was to assess the degree to which the chemical composition of the zircon (i.e., the presence of light-absorbing impurities such as REE) affects the coupling of the laser beam to the sample. **Figure 9** shows the ablation rates measured for the synthetic samples after laser ablation using 125 laser pulses fired at a repetition rate of 5 Hz and a laser fluence of 2.5 J cm^{-2}. It can be seen that there is a significant variation in the rate of ablation between the undoped zircon and the crystals doped with individual and multiple REE^{3+} and P^{5+}, with the undoped zircon showing the lowest and the Gd-, Dy-, Er-, Yb-, Y- and P-doped zircon (high doping level) showing the highest laser penetration rate. Generally, there are no significant variations in ablation rates between samples doped with a single REE. Nevertheless, the Dy-doped crystals seem to ablate at a slightly lower rate than the others, likely due to differences in the optical absorption of the laser light by the Dy-doped crystals.

Figure A4 in Appendix 2 shows the measured ablation rates as a function of the abundance of each single dopant determined by LA-ICP-MS. No correlation is observed between ablation rates and the presence of an individual REE or Hf in the zircon structure. From this, it is clear that the occurrence of a single light-absorbing element alone is not sufficient to cause the variations in the observed ablation behaviour. **Figure 10** shows measured ablation rate values as a function of P content, the amount of *Zr site* cations (i.e., Zr, REEs and Hf), and the Zr/Si intensity ratios obtained by LA-ICP-MS. There is a slight positive correlation in those three cases. Although not very significant, these trends suggest that the laser penetration rate is somewhat dependent on the degree of ion substitution into the *Zr site* by REEs and Hf, and/or into the *Si site* by P.

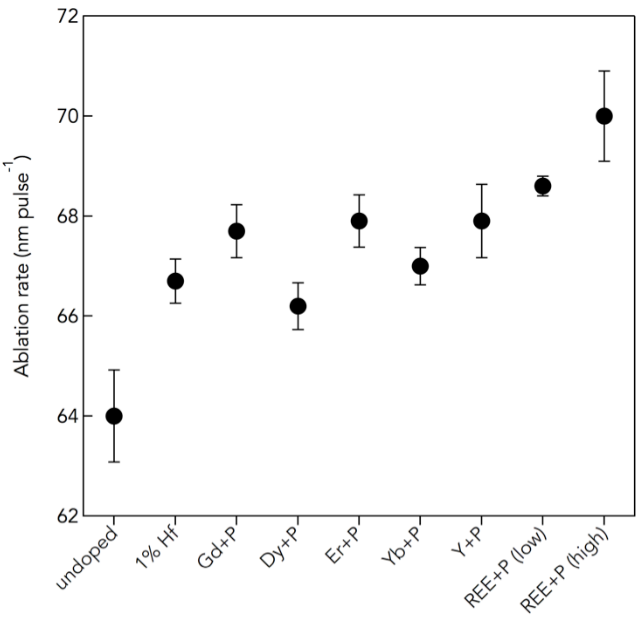

Figure 9 Ablation rates obtained for synthetic zircon crystals: undoped, Hf-doped, Gd^{3+}-and P-doped, Dy^{3+}-and P-doped, Er^{3+}-and P-doped, Yb^{3+}-and P-doped, Y^{3+}- and P-doped zircon crystals, as well as zircon crystals doped with Gd^{3+}, Dy^{3+}, Er^{3+}, Yb^{3+}, Y^{3+}-and P in two different doping levels. Uncertainties represent 2SE of the pit depth measurements (n = 6).

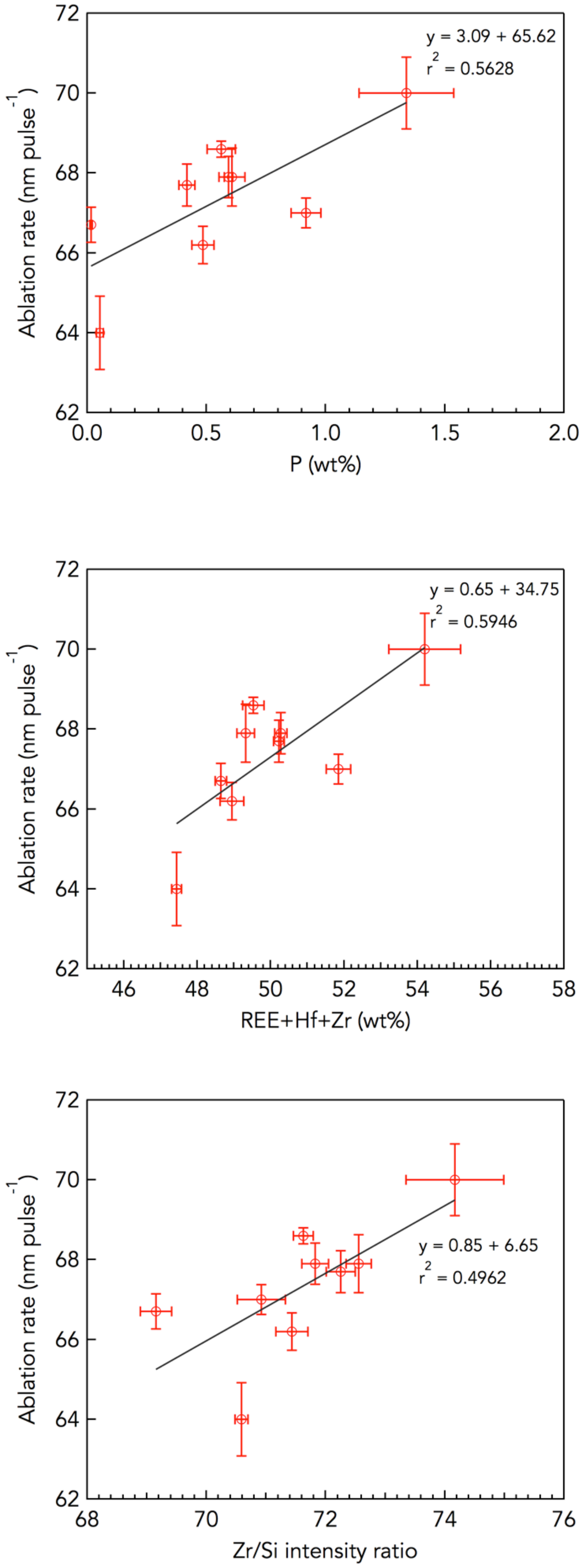

Figure 10 Ablation rate as a function of P (top), Zr-site cations (middle), and Zr/Si intensity ratio (bottom) for the synthetic crystals. Zr-site cations refer to Zr and cations that occupy Zr sites in the zircon structure, such as Y^{3+}, REE^{3+} and Hf. Uncertainties represent 2SE of the mean (n = 6).

3.3. Part III: Crystallographic orientation and crystal colour

Bulk trace element composition analyses of the Mud Tank zircon crystals show variation in elemental abundance with crystal colour (**Figure A5 in Appendix 2**). A slight increase in abundance with colour intensity is observed for Y, HREEs, Pb, Th and U. The contents of U and Th vary between ~9 – 30 µg g^{-1} and ~3 – 16 µg g^{-1}, respectively for samples MT0 to MT3. Optical cathodoluminescence imaging shows evidence of chemical zoning within the individual crystals (**Figure A6 in Appendix 2**). In situ LA-ICP-MS trace element analysis reflects the within-crystal variation, however, with only up to ~10% variation in the measured elemental abundances (**Table 1**). Raman spectra analysis of multiple spatially independent points confirmed the high degree of crystallinity as well as structural homogeneity (on the micron-scale) of the samples. Average ν_3 (SiO_4) bandwidths and frequencies are provided in **Table 2**. There is a small systematic decrease in frequency values with increasing crystal colour intensity. This minor decrease in wavenumber can be attributed to the increase in lattice width, as a result of an increasing cation substitution into the zircon structure (Nasdala et al., 2002a). The variation between all measured bandwidths (FWHM) was, however, below ± 0.15 cm^{-1} (1σ), which is well within the limits of analytical precision (± 0.5 cm^{-1}). We can therefore consider the individual Mud Tank zircon crystals as having negligible variation in (almost non-existent) accumulated radiation damage.

Table 1 LA-ICP-MS trace element composition of the Mud Tank crystals (µg g^{-1}, n = 30)

	MT0		MT1		MT2		MT3	
	Mean (%RSE)		Mean (%RSE)		Mean (%RSE)		Mean (%RSE)	
Y	30.9	(6.8)	60.3	(3.8)	66.8	(2.1)	101	(5.7)
Ce	0.43	(3.7)	0.72	(3.6)	0.82	(2.7)	0.9	(8.4)
Tb	0.32	(6.2)	0.90	(5.1)	1.1	(2.2)	1.2	(10.5)
Dy	3.7	(6.5)	8.5	(3.7)	9.8	(2.2)	13.0	(8.2)
Ho	1.2	(7.6)	2.4	(4.0)	2.7	(2.2)	4.0	(6.1)
Er	4.6	(7.7)	8.5	(5.0)	9.3	(2.2)	14.9	(5.2)
Tm	0.86	(7.6)	1.4	(4.8)	1.6	(2.4)	2.6	(4.7)
Yb	7.2	(7.5)	11.5	(5.3)	12.4	(2.0)	20.5	(4.3)
Lu	1.2	(7.6)	1.8	(5.6)	1.9	(2.4)	3.1	(4.1)
Hf	10897	(0.5)	9397	(0.9)	9359	(0.4)	9692	(1.1)
Pb	1.4	(7.5)	2.2	(6.2)	2.7	(2.9)	3.6	(6.6)
Th	3.8	(8.0)	7.9	(5.8)	9.7	(3.4)	12.2	(9.4)
U	9.6	(7.5)	16.1	(6.4)	19.0	(3.2)	26.1	(5.7)
Σ Zr-site (wt%)	1.10	(0.5)	0.95	(0.9)	0.95	(0.4)	0.99	(1.2)

EBSD crystallographic analysis revealed that crystal orientations within each sample, relative to the analysis surface, are reasonably homogeneous. Slight orientation variations within individual crystal sections (≤ 2°) were detected during electron backscatter pattern (EBSP) calculations. These variations in orientation are associated with small scratches on the sample surface that were not removed during polishing. Crystal orientation data are summarized in **Table 2**. The analysis showed that not all the crystal sections had been mounted in the ideal orientation with respect to the direction of the incident laser beam (perpendicular to the sample surface). The misorientation angles between the target crystallographic planes and the analysis surface are provided in **Table 2**.

Table 2 Relevant Raman parameters and EBSD data for the Mud Tank zircon crystals

Sample	Raman data [v_3 (SiO_4) band]		Crystal section	EBSD data		
	FWHM (cm^{-1})[a]	Raman shift (cm^{-1})[a]		c-axis (°)[b]	Target crystallographic plane[c]	Crystal plane misorientation[d] (°)
MT0	2.6 ± 0.1	1008.1 ± 0.2	MT0a	100.7	(010)	10.7
			MT0b	173.6	(001)	6.4
MT1	2.7 ± 0.1	1007.9 ± 0.2	MT1a	91.3	(010)	1.3
			MT1b	177.7	(001)	2.3
MT2	2.7 ± 0.1	1007.8 ± 0.1	MT2a	90.9	(010)	0.9.
			MT2b	34	(001)	34
MT3	2.9 ± 0.1	1007.5 ± 0.1	MT3a	91.9	(010)	1.9
			MT3b	149	(001)	31

[a]Uncertainties refer to the reproducibility of the Raman determinations performed on at least four spatially independent points (expressed as 1SD)
[b]Angle between crystal c-axis and vertical (z) axis of the sample surface.
[c]Target crystallographic plane at the analysis surface.
[d]Angle between the target crystallographic plane and the sample surface.

Ablation pit depths, measured for pits ablated using 40 μm spot size, laser fluence of ~2 J cm^{-2} and a laser repetition rate of 5 Hz, were used to calculate the ablation rates of each Mud Tank crystal section. Laser ablation rate data for all the crystal sections are provided in **Figure 11**. The data show that there is a variation in ablation rate between crystals which is, however, not strictly proportional to zircon colour. In addition, there is a slight variation in ablation rate with crystal orientation for MT1, MT2 and MT3 zircons. Crystal sections for which their c-axes are oriented close to parallel with the incident laser beam, i.e., MT1b, MT2b and MT3b, show lower rates of ablation compared to the crystal sections for which their c-axes are oriented perpendicular to the direction of the laser beam, i.e., MT1a, MT2a and MT3a. However, sample MT0 shows no clear dependence on the crystal orientation.

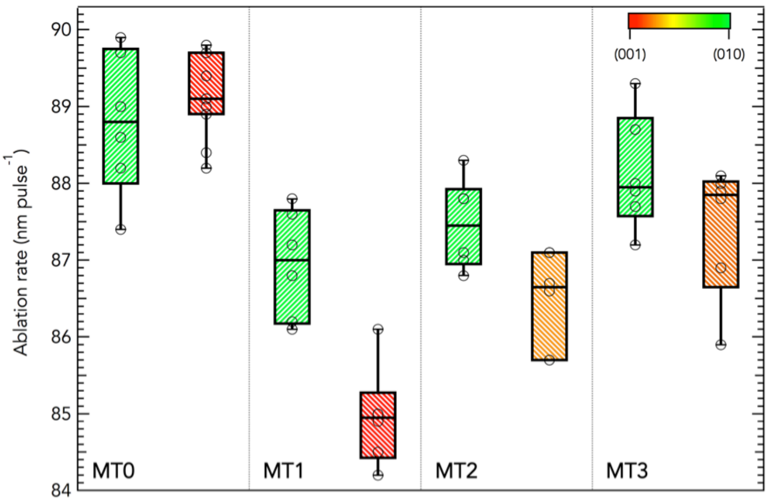

Figure 11 Ablation rates measured for the Mud Tank zircon crystals as a function of crystallographic orientation. The colour scale from red to green indicates the relative proximity of the crystallographic planes (001) and (010), respectively, to the sample surface. Data are shown as box-and-whisker plots. Open circles correspond to individual measurements; horizontal bars indicate the median; boxes span the respective interquartile; whiskers extend to the minimum and maximum measured values. Variation in ablation rates with crystal orientation is not consistent for every zircon crystal (see text for further discussion).

To evaluate the relationship between apparent $^{206}Pb/^{238}U$ age and ablation rates, measured $^{206}Pb/^{238}U$ ages are plotted in **Figure 12** by crystal sample and orientation in a manner analogous to **Figure 11**. Systematic $^{206}Pb/^{238}U$ age biases are observed between sections of the different crystals, which are well correlated with ablation rate determinations. However, while small differences in measured $^{206}Pb/^{238}U$ ages can be detected for the sections analysed in different crystal orientations (**Figure 12**), these differences agree mostly to within internal error. The age corresponding to the weighted mean of 119 analyses is 720.7 ± 3.1 Ma (2SE), which is outside the uncertainty of the TIMS age (i.e., 731 ± 0.49 Ma; Horstwood et al., 2016). The good correlation between laser ablation rates and apparent LA-ICP-MS $^{206}Pb/^{238}U$ ages suggest that the age data obtained in this study are systematically underestimated by some degree as a result of differences in ablation behaviour between the zircon reference material (i.e., 91500 zircon) and the various Mud Tank zircon crystals.

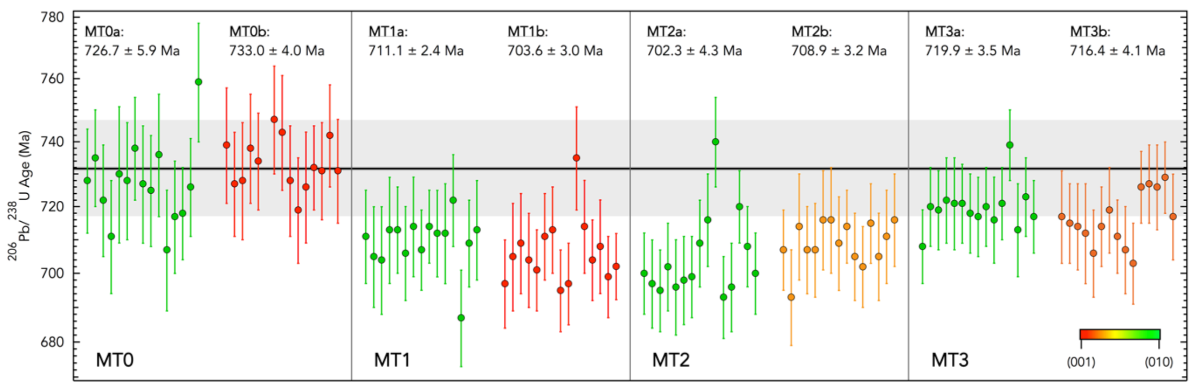

Figure 12 Plot of individual $^{206}Pb/^{238}U$ ages (circles) measured for the Mud Tank crystals during a single analytical session (weighted mean 720.7 ± 3.1 Ma, 2SE, n = 119). The 91500 zircon was used as primary reference material for age calibration. Error bars show the internal precision of the measurements (expressed as 2SE). Solid black line and dark grey area show the TIMS age and its uncertainty (731.65 ± 0.49 Ma; Horstwood et al., 2016), respectively. A light grey area corresponding to a ±2% TIMS age offset is provided as reference. For better comparison with the reported ablation rates, LA-ICP-MS $^{206}Pb/^{238}U$ ages are categorised by sample (MT0 to MT3)

and crystallographic orientation (colour scale from red to green) similarly to **Figure 11**. The offset between the weighted mean $^{206}Pb/^{238}U$ age of each crystal section ranges from 0.5% to 5% and is directly proportional to the differences in measured ablation rates.

4. Discussion

4.1. Role of radiation-induced structural defects on the ablation behaviour of natural zircon

Based on the overall positive linear correlation between zircon ablation rate and radiation damage, it is reasonable to assume that quantification of the total accumulated radiation-induced damage (i.e., using Raman spectroscopy) can be used as a proxy for laser drill rate into natural zircon. However, there are practical constraints to this approach, which are imposed by the limited accessibility to the Raman spectroscopy technique among the U-Pb geochronology community, and the potential time constraints involved. Whereas it might be conceivable to monitor radiation damage for a few representative grains in a study of a magmatic zircon population, it would clearly be unfeasible to achieve the same level of characterisation for a suite of detrital zircon grains. Alternatively, there is a simplified mathematical approach to quantifying the number of alpha particles released over time during the decay of U and Th, which may correlate with the extent of structural distortion experienced by a zircon matrix (Murakami et al., 1991). Here, the self-irradiation dose for each zircon is quantified as the total alpha-fluence (i.e., D_α, number of alpha-decay events per gram), which is given by:

$$D_\alpha = 8 \times \frac{c_U \times N_A \times 0.9928}{M_{238} \times 10^6} \times \left(e^{\lambda_{238} t} - 1\right) + 7 \times \frac{c_U \times N_A \times 0.0072}{M_{235} \times 10^6} \times \left(e^{\lambda_{235} t} - 1\right) + 6 \times \frac{c_{Th} \times N_A}{M_{232} \times 10^6} \times \left(e^{\lambda_{232} t} - 1\right) \quad (2)$$

where C_U and C_{Th} are the U and Th abundances (in µg g^{-1}), respectively; N_A is Avogadro's number; M_{238}, M_{235} and M_{232} are the molecular weights of the parent isotopes; λ_{238}, λ_{235} and λ_{232} are the corresponding decay constants; and t is the crystallization age of the zircon.

One restriction to this mathematical approach is that it only provides a sensible estimation of the radiation-induced structural damage if no significant damage annealing has occurred since the zircon crystallised (Nasdala et al., 2001; Palenik et al., 2003). Considering the latter, it is important to further assess the applicability of the calculated total alpha-fluence (i.e., D_α) as a proxy for laser drill rate. Here we use the approach provided by Nasdala et al. (2001) to provide insight into the correlation between the actual degree of metamictisation (provided by Raman spectroscopy) and the computed self-irradiation dose for natural zircon. This approach is based on the comparison between the correlation estimated in this study (i.e., ν_3 (SiO_4) FWHM *versus* D_α) and a calibration curve previously obtained for zircon matrices that have not experienced annealing during their geological history (see Nasdala et al., 2001). The aim is to easily identify zircon samples that have not accumulated their radiation damage completely, and to evaluate the effects that natural annealing has on the ν_3 (SiO_4) FWHM values, but most importantly on the ablation behaviour of zircon. To this end we have quantified the self-irradiation dose of our zircon reference materials (i.e., D_α) using **Eq. (2)** assuming a crystallisation age (t in the equation) equivalent to their accepted TIMS U-Pb age. **Figure 13** shows the increase in measured FWHM values as a function of the calculated total alpha-fluence. It can be seen that most data pairs follow the same general trend and plot within the calibration band provided by Nasdala et al. (2001) for zircon matrices that have not experienced significant natural annealing and thus are thought to have stored their radiation damage completely. Nearly all data pairs for the QGNG zircon plot slightly below the calibration line, which indicates that the measured bandwidths (ν_3 (SiO_4) FWHM) are rather lower than would be expected from their U-Th content and crystallization age. This observation points to an incomplete storage of the accumulated radiation damage by the QGNG zircon crystals (Nasdala et al., 2001). This finding is in good agreement with previous evidence for the partial loss of radiogenic Pb in QGNG zircon crystals (Black et al., 2003).

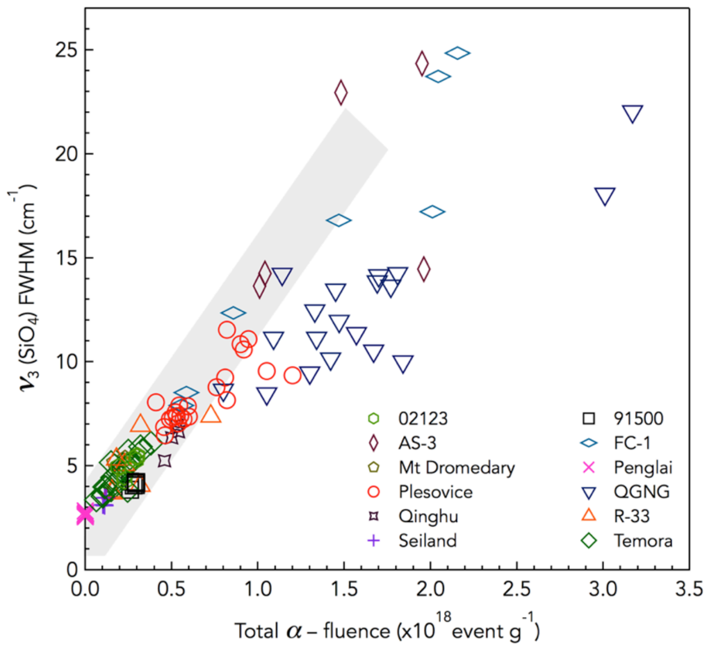

Figure 13 FWMH of the ν_3 (SiO_4) Raman band as a function of the calculated total alpha-fluence for our zircon samples. The grey area corresponds to the calibration field reported by (Nasdala et al., 2001) for zircon matrices that have accumulated their radiation damage almost completely. Note that most data pairs follow the general trend of increasing degree of radiation damage (i.e., ν_3 (SiO_4) FWHM) with increasing self-irradiation dose and plot very close to the calibration line, except for the QGNG zircon. This indicates incomplete damage accumulation for the QGNG zircon due to partial annealing.

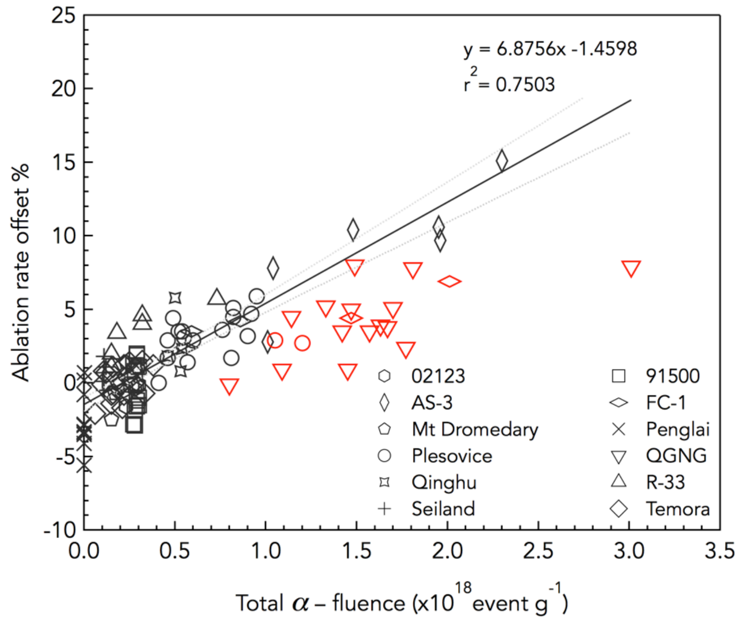

Figure 14 Ablation rate offset percent as a function of the total alpha fluence. The best-fit line was generated using data pairs for zircon matrices that are thought not to have undergone natural annealing (black). Data pairs for zircon grains that have undergone partial structural reconstitution from a natural annealing event are shown in red. Note that these zircon specimens show rather lower ablation rates to what it is expected from their calculated self-irradiation dose.

Bearing in mind that thermal treatment in the laboratory reduces to some extent the ablation rate of the annealed samples (Marillo-Sialer et al., 2014), we have no reason to think that the damage reconstitution caused by a natural thermal event (long-term, low-temperature annealing) would have any different effect. We would expect, therefore, an overall reduction in ablation rates for the QGNG zircon compared to that predicted from the self-irradiation dose calculated from its U and Th contents. In order to evaluate this assumption, **Figure 14** shows the linear trend obtained when plotting drill rates as a function of the total alpha-fluence for zircon matrices whose data pairs lie within the calibration band in **Figure 13**. Data for the QGNG zircon are shown for comparison. It can be seen that data pairs for the QGNG zircon do not follow the trend of increasing drill rate with total alpha-fluence defined by the other zircon reference materials. What is apparent from the above results is that the fact that the QGNG zircon has undergone partial natural annealing, and thus partial structural reconstitution, affects its ablation behaviour and prevents the use of the calculated total alpha-fluence (i.e., D_α) as proxy for its laser drill rate.

Consequently, the positive correlation between radiation damage and ablation rates observed for well-crystallised to highly metamict zircon matrices (see **Figure 4**) can be assumed to be a result of the average structural distortions in the zircon matrix. Based on this assumption, laser ablation rates are interpreted to reflect the associated property changes in partially metamict matrices, such as decreased birefringence, enhanced chemical reactivity, reduced mechanical resistance and the general decrease in crystal density and compressibility (Woodhead et al., 1991; Ewing et al., 2003 and references therein). The comparison between thermal annealing of samples done in the laboratory at two different temperatures for different heating times, i.e., 850 °C for 48 h and 1000 °C for 36 h, suggests that incomplete reconstitution of the crystal structure for partially to highly metamict zircon matrices treated at 850 °C is responsible for the remaining differences in ablation rates observed for different samples in Marillo-Sialer et al. (2014). The degree of radiation damage was found to be still significant for the QGNG and Plešovice zircons after annealing upon heat treatment at 850 °C, which is in agreement with previous findings of incomplete recovery of radiation damage in moderate to highly metamict matrices for annealing at temperatures lower than ~950 °C (Murakami et al., 1991; Colombo et al., 1999; Zhang et al., 2000a; Geisler et al., 2001; Geisler, 2002; Nasdala et al., 2002b; Mattinson, 2005). On the other hand, heat treatment at 1000 °C caused significant recovery of the crystalline microstructure for all the treated samples. These observations are consistent with those of Mattinson (2000 , 2005), who recommends the use of an annealing temperature of 1000 °C for 48 h to guarantee significant removal of radiation damage in highly damaged materials. Moreover, it has been previously demonstrated that structural recovery and recrystallization of damaged zircon samples occurs in a multi-stage process that depends on the degree of initial damage of the samples. In heavily damaged materials, for example, the main recrystallization of amorphous zircon occurs after the amorphous material was partially decomposed into ZrO_2 and SiO_2. (Capitani et al., 2000; Zhang et al., 2000a; Geisler et al., 2001; Geisler et al., 2003b). This is in agreement with our observation that, although all the treated samples could be categorised as well-crystallised zircon (i.e., $\nu_3\,(SiO_4)$ FWHM < 5 cm^{-1}), only the annealed 02123 and 91500 zircons showed crystalline microstructures equivalent to the synthetic zircon. Nevertheless, the increased crystallinity of the reconstituted zircon matrices is thought to be responsible for the increased similarities in ablation behaviour observed among the majority of the treated samples. This homogenisation in ablation behaviour is closely associated with a decrease of approximately 2% in the scatter of U-Pb age bias (i.e., $\Delta^{206}Pb/^{238}U$ age % in **Figure 8**). This is in reasonable agreement with the increase in LA-ICP-MS U-Pb age accuracy reported for zircon after thermal treatment at 850 °C for 48 h by Allen and Campbell (2012) and Solari et al. (2015). A precise explanation for the different results obtained at those annealing conditions in this study (i.e., no U-Pb age accuracy improvement for zircon samples treated at 850 °C for 48 h) cannot be given. However, different annealing conditions, such as stepwise annealing, annealing in N_2 atmosphere, heat treatment under hydrothermal conditions, among others (Ewing et al., 2003; and references therein), have all been reported to account for differences in zircon annealing rates. The latter cannot be applied to explain the differences between the two previous studies (i.e., Allen and Campbell, 2012; Solari et al., 2015) and the present work since, in all these cases, the samples were treated in an ambient, dry atmosphere (i.e., 850 °C). Regardless of the cause leading to the differences between annealing studies, we have shown here that the success of high-temperature thermal treatment in homogenising the ablation behaviour of zircon matrices, and thus improving the LA-ICP-MS technique for U-Pb zircon dating, is highly dependent on the final microstructure of the treated samples. We recommend, therefore, that natural zircon be annealed in future LA-ICP-MS U-Pb geochronology studies using temperatures higher than ~950 °C and for 36 h or longer in order to achieve a significant reduction of structural distortions and guarantee uniform annealing performance for slightly, moderate and highly damaged zircon matrices.

4.2. Dependence of the ablation rate on the chemical composition of zircon

It is a common observation among LA-ICP-MS users that some minerals which are not easily ablated, such as quartz or fluorite, tend to become easier to ablate with increasing trace element content. The underlying principles behind this observation are, however, not well understood. It is thought that the occurrence of UV laser light-absorbing trace elements, such as the REE, enhance the coupling between the laser radiation and the target material in that they increase the efficiency with which the incident laser radiation is absorbed (Götze and Möckel, 2012).

A wide variety of elements are reportedly present in natural zircon in minor to trace amounts. From those, Hf, REEs, P, U and Th occur in relatively high abundances (Hoskin and Schaltegger, 2003). Certainly, due to their electronic structure, the REE^{3+} have electronic energy levels in the $4f^N$ and $4f^{N-1}5d$ configurations that allow electronic transitions through absorption of UV laser light (Liu and Jacquier, 2006). Increased absorption due to the occurrence of certain trace elements has been reported to affect the ablation behaviour of glass by decreasing the laser penetration rate during ablation with a 266 nm Nd:YAG laser (Horn et al., 2001; Weis et al., 2005). The latter agrees with theoretical expectations regarding laser-matter interactions, in that an increased absorption of the laser light at the target surface will decrease the penetration of the laser beam into the bulk of the sample (von Allmen and Blatter, 1995). The results of our ablation rate determinations for the various synthetic crystals, however, do not show this pattern of decreasing ablation rate with increasing trace element abundance (see **Figure 9**). On the contrary, the 193 nm excimer laser seems to penetrate at a lower rate into the undoped zircon crystals, than into the doped specimens. This suggests that an increased absorption of laser light due solely to the presence of trace impurities does not play a significant role, or at least not a direct role, in producing the variations in ablation behaviour observed for the synthetic samples in this study. This observation agrees, to some extent, with early evidence that showed no differences in ablation rates between silicate glasses of the NIST SRM 61X series, i.e., NIST 612 (low trace element content) and NIST 610 (high trace element content) due to changes in the degree of laser-light absorption by the sample during ablation with a 193 nm excimer laser (Horn et al., 2001). The fact that we do observe differences (but an increase, not a decrease) in ablation rates with increasing abundance of trace elements for the synthetic samples shows that the presence of trace impurities within the structure of crystalline zircon, or at least the occurrence of Hf, Y, and/or the REE at the concentrations studied, does have an effect on the ablation performance of 193 nm excimer lasers. From **Figure 10**, it seems that the ablation behaviour of crystalline zircon, rather than being related to the light-absorption abilities of any particular trace element, is dependent on the amount of elements that have been incorporated into the zircon structure.

It has been previously reported that, even after annealing of radiation damage, there is an enhanced susceptibility of regions in zircon crystals with high concentrations of U, Th and other trace elements to chemical attack (Mattinson, 2005). Similarly here, a greater concentration of trace element-induced structural distortions results in an enhanced susceptibility of zircon crystals to ablation (i.e., an increase in laser penetration rates). It has been previously shown by van Westrenen et al. (2004) that the structural changes arising from trace element substitution into the zircon structure (i.e., approximately 1% increase in unit-cell volume compared to that of undoped synthetic zircon) lead to changes in physical properties, specifically a decrease in elastic moduli of zircon (i.e., increase in compressibility). Given that radiation-induced damage to the zircon structure causes similar effects on the compressibility of the zircon crystals (Özkan, 1976; Chakoumakos et al., 1991; Oliver and McCallum, 1994; Salje, 2006), it is not surprising that the incorporation of trace elements into the zircon structure has the potential to affect the ablation behaviour of zircon. There are, however, two unexpected results. First, that doping levels as low as 0.6 wt%, as is the case of the Gd-and P-doped synthetic zircon, can vary the ablation rate of zircon by ~5.5% relative to the undoped specimen. Second, that the incorporation of Hf into the zircon structure causes the same variation in ablation behaviour as the incorporation of, for example, the REE, i.e., an increase in ablation rates. Since hafnon ($HfSiO_4$) has a smaller unit-cell volume than zircon, it is likely that the Hf-doped zircon crystals have a slightly smaller unit-cell volume, and therefore slightly larger elastic moduli, than the undoped zircon crystals (van Westrenen et al., 2004). Thus, it would have been expected that Hf-doped crystals would show ablation rates that are lower than those measured for pure, undoped zircon, and this contradicts our experimental observations. At present, no definitive explanation for the increase in zircon ablation rates with Hf-content can be given. It should nevertheless be taken into account that natural zircon generally contains minor amounts of Hf (with reported abundances of as low as ~0.2 wt.% and up to ~12 wt.%, but more typically the Hf concentration ranges between 0.5 and 3 wt.%) and less than 1 wt.% of REEs (Hoskin and Schaltegger, 2003 and references therein). Therefore, any variations in the ablation behaviour between various natural crystalline zircon samples as a result of their chemistry are likely to be related to differences in their Hf content.

We note that the observed decrease in elastic moduli of zircon due to cation substitution is generally much less than the decrease in elastic moduli of zircon crystals arising from radiation damage (Özkan, 1976; Oliver and McCallum, 1994; Salje, 2006). For that reason, radiation-induced damage to the zircon structure still plays the major role in determining the ablation behaviour of natural zircon. Nonetheless, the results obtained in this part of the study clearly show that the physical changes associated with the increasing structural strain resulting from the incorporation of minor and/or trace elements can cause an increase in ablation rates. The latter may provide an explanation for the rather large scatter in ablation rates observed for natural, crystalline zircon matrices where the effects of radiation damage on the structure are negligible (refer to **Figure 4**).

4.3. Effect of the crystallographic orientation on the ablation behaviour of zircon

Although some crystalline minerals show distinctly different optical and mechanical properties on different crystallographic planes, the effect of this crystallographic anisotropy on their ablation behaviour has been poorly investigated. In the case of alkali feldspars, Mikova et al. (2009) reported significant differences in the ablation behaviour of albite ($NaAlSi_3O_8$) with crystallographic orientation during sampling using a 213 nm Nd:YAG laser. Similarly, differences in ablation behaviour, and associated variations in elemental fractionation, have been observed for quartz when ablated in different crystallographic planes using a 193 nm ArF excimer laser (Götze and Möckel, 2012). In regard to *in situ* U-Pb geochronology, crystallographic orientation has been reported as associated with variations in $^{206}Pb/^{238}U$ ratios measured in baddeleyite by high-resolution ion microprobe (Wingate and Compston, 2000), and in rutile by secondary ion mass spectrometry (Taylor et al., 2012). However, no evidence for crystal orientation-related $^{206}Pb/^{238}U$ age bias has been reported for zircon during *in situ* microanalysis (Wingate and Compston, 2000; Black et al., 2004).

In particular, difficulties related to the availability of well-characterised zircon crystals with a relatively homogeneous U-Pb ratio at the intra- and inter-grain scale, that are large enough to allow sectioning in different crystallographic planes, have prevented a comprehensive analysis of the effects of crystallographic orientation on the ablation behaviour of zircon and associated U-Pb age bias. We attempted to overcome these limitations by analysing multiple crystals of the Mud Tank zircon. FWHM and wavenumber values of the $\nu_3\,(SiO_4)$ Raman band obtained for the Mud Tank zircon crystals (**Table 2**) are very close to those reported for synthetic zircon by Nasdala et al. (2004). For that reason, they can be regarded as highly crystalline zircon matrices having accumulated no or insignificant radiation damage in their structure. We can assume, therefore, that any differences in ablation behaviour observed between individual Mud Tank crystals or crystal sections are related to causes other than radiation-induced structural damage.

We observed a variation of up to ~5% between average ablation rate values of individual sections of the Mud Tank crystals (**Figure 11**). The largest variation in ablation rates occurs between sections oriented close to the (001) plane of two different crystals, i.e., MT0 and MT1. This suggests that this variation may be due to differences in chemical composition between crystals rather than to any crystallographic effect. Indeed, there seems to be a correlation between the amount of elements substituting on the *Zr site* (**Table 1**) and the average ablation rate of each Mud Tank crystal. Nonetheless, there is an apparent decrease in ablation rates for the crystal sections oriented close to the (001) crystallographic plane compared to those obtained for crystal sections oriented parallel to (010) for samples MT1, MT2 and MT3, which does not seem to be strictly associated with the crystal chemistry. However, in all three cases the variation in average ablation rate for the two sections of a same zircon crystal (e.g., MT3a and MT3b) are within error of the ablation rate determinations. The ablation rates measured for both sections of sample MT0 (i.e., MT0a oriented close to the (010) plane and MT0b oriented close to the (001) plane) are indistinguishable from each other. All these observations suggest that if there is a dependence of ablation behaviour on the crystal orientation of zircon, this is not strong.

Figure 15 shows the correlation between $^{206}Pb/^{238}U$ LA-ICP-MS age bias and the offset in measured ablation rates. It can be seen that the apparent U-Pb age bias correlates significantly with measured ablation rates (see also **Figure 12**). Such a correlation would suggest that, if there is any variation in zircon $^{206}Pb/^{238}U$ LA-ICP-MS ratios with crystallographic orientation this would be, at least to a considerable extent, attributable to differences in the ablation behaviour between crystals. We assume, therefore, that any laser-induced matrix effects related to the crystallographic orientation of a zircon crystal relative to the incident laser beam is not related to thermally-induced diffusion processes such as those described for alkali feldspars by Mikova et al. (2009). In addition, the apparent differences in ablation rates with crystal orientation observed for MT1, MT2 and MT3, seem to cause variations in the $^{206}Pb/^{238}U$ ages of up to ~1%. This variation is much less significant than the changes in ablation rates caused by differences in chemical composition between the Mud Tank zircon crystals (~4%). For that reason, we suggest that crystallographic orientation does not play a major role in defining the ablation behaviour of zircon relative to the much stronger variations associated to increased structural strain and distortion resulting from the incorporation of minor- and trace elements into the zircon structure and from radiation-induced damage, respectively.

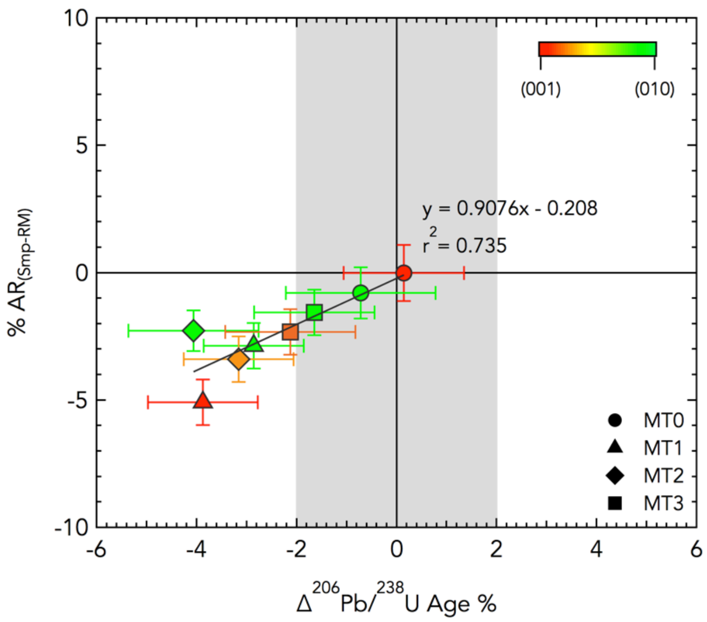

Figure 15 Ablation rate percent offset ($\Delta AR_{(Smp\text{–}RM)}$) *versus* $^{206}Pb/^{238}U$ age percent offset ($\Delta^{206}Pb/^{238}U$ *Age*) for the Mud Tank zircon crystals. Ablation rate offsets were calculated relative to the ablation rate of the 91500 zircon reference material used for age calibration. The colour scale from red to green indicates the relative proximity of the crystallographic planes (001) and (010), respectively, to the sample surface.

5. Conclusions and recommendations

Accurate identification and refinement of the multiple variables affecting the rate of material removal by the laser is a first step towards the adequate correction for the systematic LA-ICP-MS U-Pb age bias observed between zircon matrices, and could potentially lead to a significant decrease of measurement uncertainty in LA-ICP-MS age determinations. Differences in the degree of metamictisation between natural zircon samples seem to play a dominant role in defining the observed variation in ablation characteristics for well crystallised to highly metamict matrices, consistent with prior observations by Steely et al. (2014). Additionally, our results indicate that samples with a well-crystallized structure (ν_3 (SiO_4) FWHM ≤ 5 cm^{-1}) show differences in ablation rates that are related to the increasing cation substitution into the zircon structure (and associated changes in mechanical properties; e.g., decrease in elastic moduli), and to a much lesser extent (almost negligible) to the crystallographic orientation. As a result of this, crystalline zircon samples show significant variations in ablation rates that are not strictly correlated to their degree of accumulated radiation damage. It follows that, in general, the increase in laser penetration rate is associated with a decrease in the ability of a zircon crystal to withstand the thermo-mechanical stress applied during laser irradiation, which is a consequence of a weakening of interatomic bonds induced by increasing cation substitution and radiation damage.

Our Raman data demonstrate that the reduction in ablation rates observed for thermally treated samples is proportional to the degree of structural reconstitution achieved after annealing. It was shown that differences in ablation rate between zircon matrices after annealing at 850 °C for 48 h were caused by the incomplete structural reconstitution of samples which were originally moderate to highly metamict. In contrast, equivalent ablation rates were measured between different zircon matrices after thermal treatment at 1000 °C for 36 h, regardless of their initial structural state.

Taken together, these experiments provide a roadmap for improvements in the accuracy of U-Pb age determinations by LA-ICP-MS. Our studies confirm the usefulness of annealing to increase the similarities in ablation behaviour between zircon matrices, and thus decrease the predominant matrix-related bias. Wherever possible, annealing should be undertaken as a prerequisite to laser ablation U-Pb geochronology. We note, however, that a significant improvement in U-Pb age determination is observed only after all zircon materials (reference *and* unknown) have reached a high degree of structural reconstitution due to annealing with $\nu_3(SiO_4)$ FWHM values of 5 cm^{-1} or lower. We recommend therefore that annealing temperatures of over 950 °C are used in order to avoid incomplete structural reconstitution of metamict to highly metamict zircon samples. If prior annealing is not available, it may be possible to make corrections for differential ablation behaviour due to accumulated radiation damage either by measurement of Raman spectra (only feasible for a limited number of grains representative of magmatic populations) or by calculation of accumulated radiation dose from measured U and Th contents (subject to the caveats in this method noted previously). In the absence of such strategies, matching the primary reference material to the unknowns in terms of accumulated radiation damage will certainly likely increase accuracy to some extent, although not to the levels achievable with thermal annealing. In addition, to better mitigate the laser-induced matrix effects, closer matching of the total content of minor and trace elements between annealed zircon reference materials and samples is likely to be advantageous. Samples with unusual Hf or trace element contents may exhibit unexpected ablation characteristics resulting in the potential for increased matrix-related age inaccuracy.

6. Acknowledgments

The authors would like to acknowledge B. Johnson and S. Rubanov for technical assistance with Raman spectrometry and HR-TEM analyses, respectively. X-H. Li is thanked for providing the Qinghu zircon. M. Horstwood and an anonymous reviewer are thanked for providing comments that helped improve the quality of this manuscript. This work was supported by an Albert Shimmins Postgraduate Award from the University of Melbourne to EMS, and an NSERC Discovery grant to JMH.

7. References

Abrarov, S.M. and Quine, B.M., 2011, Efficient algorithmic implementation of the Voigt/complex error function based on exponential series approximation. *Applied Mathematics and Computation*, 218(5): 1894-1902.

Allen, C. and Campbell, I., 2012, Identification and elimination of a matrix-induced systematic error in LA–ICP–MS 206Pb/238U dating of zircon. *Chemical Geology*, 332-333: 157-165.

Ando, A., 1984, New silicate rock reference materials issued from the Geological Survey of Japan, 1984. *Geochemical Journal*, 18: 215-216.

Babechuk, M., Kamber, B., Greig, A., Canil, D. and Kodolanyi, J., 2010, The behaviour of tungsten during mantle melting revisited with implications for planetary differentiation time scales. *Geochimica et Cosmochimica Acta*, 74(4): 1448-1470.

Bergman, L., Alexson, D., Murphy, P. and Nemanich, R., 1999, Raman analysis of phonon lifetimes in AIN and GAN of wurtzite structure. *Physical Review B*, 59(20): 12977-12982.

Black, L., Kamo, S., Williams, I., Mundil, R., Davis, D., Korsch, R. and Foudoulis, C., 2003, The application of SHRIMP to Phanerozoic geochronology; a critical appraisal of four zircon standards. *Chemical Geology*, 200(1-2): 171-188.

Black, L., Kamo, S., Allen, C., Davis, D., Aleinikoff, J., Valley, J., Mundil, R., Campbell, I., Korsch, R., Williams, I. and Foudoulis, C., 2004, Improved 206Pb/238U microprobe geochronology by the monitoring of a trace-element-related matrix effect; SHRIMP, ID–TIMS, ELA–ICP–MS and oxygen isotope documentation for a series of zircon standards. *Chemical Geology*, 205: 115-140.

Capitani, G.C., Leroux, H., Doukhan, J.C., Ríos, S., Zhang, M. and Salje, E.K.H., 2000, A TEM investigation of natural metamict zircons: structure and recovery of amorphous domains. *Physics and Chemistry of Minerals*, 27.

Chakoumakos, B.C., Oliver, W.C., Lumpkin, G.R. and Ewing, R., 1991, Hardness and elastic modulus of zircon as a function of heavy-particle irradiation dose: I. In situ α-decay event damage. *Radiation Effects and Defects in Solids*, 118: 393-403.

Colombo, M., Chrosch, J. and Salje, E.K.H., 1999, Annealing Metamict Zircon: A Powder X ray Diffraction Study of a Highly Defective Phase. *Journal of the American Ceramic Society*, 82(10): 2711-2716.

Eggins, S., Kinsley, L. and Shelley, J., 1998, Deposition and elemental fractionation processes during atmospheric pressure laser sampling for analysis by ICP-MS. *Applied Surface Science* 127-129: 278-286.

Eggins, S.M., Woodhead, J.D., Kinsley, L.P.J., Mortimer, G.E., Sylvester, P., McCulloch, M.T., Hergt, J.M. and Handler, M.R., 1997, A simple method for the precise determination of 40 trace elements in geological samples by ICPMS using enriched isotope internal standardisation. *Chemical Geology*, 134(4): 311-326.

Evans, N.J., McInnes, B.I.A., McDonald, B., Danišík, M., Becker, T., Vermeesch, P., Shelley, M., Marillo-Sialer, E. and Patterson, D.B., 2015, An in situ technique for (U–Th–Sm)/He and U–Pb double dating. *Journal of Analytical Atomic Spectrometry*, 30(7).

Ewing, R., Meldrum, A., Wang, J., Weber, W. and Corrales, R., 2003, Radiation Effects in Zircon. In: Hanchar, J. and Hoskin, P. (eds.), Zircon. Mineralogical Society of America, Washington, DC, pp. 387-425.

Finch, R. and Hanchar, J., 2003, Structure and chemistry of zircon and zircon-group minerals In: Hanchar, J.M. and Hoskin, P. (eds.), Zircon. Mineralogical Society of America, Washington, DC, pp. 1-21.

Finch, R.J., Hanchar, J.M., Hoskin, P.W.O. and Burns, P.C., 2001, Rare-earth elements in synthetic zircon: Part 2. A single-crystal X-ray study of xenotime substitution. *American Mineralogist*, 86: 681-689.

Fisher, C., Hanchar, J., Samson, S., Dhuime, B., Blichert-Toft, J., Vervoort, J. and Lam, R., 2011, Synthetic zircon doped with hafnium and rare earth elements: A reference material for in situ hafnium isotope analysis. *Chemical Geology*, 286: 32-47.

Geisler, T., Pidgeon, R., van Bronswijk, W. and Pleysier, R., 2001, Kinetics of thermal recovery and recrystallization of partially metamict zircon: a Raman spectroscopic study. *European Journal of Mineralogy*, 13: 1163-1176.

Geisler, T., 2002, Isothermal annealing of partially metamict zircon: evidence for a three-stage recovery process. *Physics and Chemistry of Minerals*, 29(6): 420-429.

Geisler, T. and Pidgeon, R.T., 2002, Raman scattering from metamict zircon: comments on "Metamictisation of natural zircon: accumulation versus thermal annealing of radioactivity-induced damage" by Nasdala et al. 2001 (Contribution to Mineralogy and Petrology 141: 125-144). *Contributions to Mineralogy and Petrology*, 143(6): 750-755.

Geisler, T., Rashwan, A.A., Rahn, M.K.W., Poller, U., Zwingmann, H., Pidgeon, R.T., Schleicher, H. and Tomaschek, F., 2003a, Low-temperature hydrothermal alteration of natural metamict zircons from the Eastern Desert, Egypt. *Mineralogical Magazine*, 67(3): 485-508.

Geisler, T., Zhang, M. and Salje, E.K.H., 2003b, Recrystallization of almost fully amorphous zircon under hydrothermal conditions: An infrared spectroscopic study. *Journal of Nuclear Materials*, 320.

Götze, J. and Möckel, R. (eds.), 2012, Quartz: Deposits, mineralogy and analytics. *Springer Geology*, Springer-Verlag Berlin Heidelberg, 360 p.

Hanchar, J. and Finch, R., 2001, Rare earth elements in synthetic zircon: Part 1. Synthesis, and rare earth element and phosphorus doping. *American Mineralogist*, 86: 667-680.

Holland, H. and Gottfried, D., 1955, The effect of nuclear radiation on the structure of zircon. *Acta Crystallographica*, 8: 291-300.

Horn, I., Guillong, M. and Günther, D., 2001, Wavelength dependant ablation rates for metals and silicate glasses using homogenized laser beam profiles - implications for LA-ICP-MS. *Applied Surface Science*, 182(1-2): 91-102.

Horstwood, M.S.A., Košler, J., Gehrels, G., Jackson, S., McLean, N., Paton, C., Pearson, N., Sircombe, K., Sylvester, P., Vermeesch, P., Bowring, J., Condon, D.J. and Schoene, B., 2016, Community ‐ Derived Standards for LA ‐ ICP ‐ MS U ‐ Th ‐ Pb Geochronology ‐ Uncertainty Propagation, Age Interpretation and Data Reporting. *Geostandards and Geoanalytical Research*, DOI: 10.1111/j.1751-908X.2016.00379.x.

Hoskin, P. and Schaltegger, U., 2003, The composition of zircon and igneous and metamorphic petrogenesis. In: Hanchar, J.M. and Hoskin, P. (eds.), Reviews in Mineralogy and Geochemistry. The Mineralogical Society of America, Washington, pp. 27- 55.

Kamber, B.S., Greig, A., Schoenberg, R. and Collerson, K.D., 2003, A refined solution to Earth's hidden niobium: implications for evolution of continental crust and mode of core formation. *Precambrian Research*, 126(289-308).

Kamber, B.S., Greig, A. and Collerson, K.D., 2005, A new estimate for the composition of weathered young upper continental crust from alluvial sediments, Queensland, Australia. *Geochimica et Cosmochimica Acta*, 69(4): 1041-1058.

Ketchum, J.W.F., Jackson, S.E., Culshaw, N.G. and Barr, S.M., 2001, Depositional and tectonic setting of the Paleoproterozoic Lower Aillik Group, Makkovik Province, Canada: evolution of a passive margin-foredeep sequence based on petrochemistry and U-Pb (TIMS and LA-ICP-MS). *Precambrian Research*, 105: 331-356.

Klötzli, U., Klötzli, E., Günes, Z. and Košler, J., 2009, Accuracy of laser ablation U-Pb zircon dating: Results from a test using five different reference zircons. *Geostandards and Geoanalytical Research*, 33(1): 5-15.

Kooijman, E., Berndt, J. and Mezger, K., 2012, U-Pb dating of zircon by laser ablation ICP-MS: recent improvements and new insights. *European Journal of Mineralogy*, 24(1): 5-21.

Košler, J., Sláma, J., Belousova, E., Corfu, F., Gehrels, G., Gerdes, A., Horstwood, M., Sircombe, K., Sylvester, P., Tiepolo, M., Whitehouse, M. and Woodhead, J., 2013, U-Pb Detrital Zircon Analysis - Results of an Inter-laboratory Comparison. *Geostandards and Geoanalytical Research*, 37(3): 243-259.

Li, X., Tang, G., Gong, B., Yang, Y., Hou, K., Hu, Z., Li, Q., Liu, Y. and Li, W., 2013, Qinghu zircon: A working reference for microbeam analysis of U-Pb age and Hf and O isotopes. *Chinese Science Bulletin*, 58.

Liu, G. and Jacquier, B., 2006, Spectroscopic properties of rare earths in optical materials. *Springer Series in Materials Science*, Springer-Verlag Berlin Heidelberg, 550 p.

Marillo-Sialer, E., Woodhead, J., Hergt, J., Greig, A., Guillong, M., Gleadow, A., Evans, N. and Paton, C., 2014, The zircon 'matrix effect': evidence for an ablation rate control on the accuracy of U–Pb age determinations by LA-ICP-MS. *Journal of Analytical Atomic Spectrometry*, 29: 981-989.

Mattinson, J., 2000, U-Pb zircon analysis by "chemical abrasion": combined high-temperature annealing of radiaiton damage and partial dissolution analysis. *Eos Trans AGU*, 8(19): S27 (GS32A-02).

Mattinson, J.M., 2005, Zircon U Pb chemical abrasion (CA-TIMS) method: combined annealing and multi-step partial dissolution analysis for improved precision and accuracy of zircon ages. *Chemical Geology*, 220(1): 47-66.

Mikova, J., Košler, J., Longerich, H., Wiedenbeck, M. and Hanchar, J., 2009, Fractionation of alkali elements during laser ablation ICP-MS analysis of silicate geological samples. *Journal of Analytical Atomic Spectrometry*, 24(9): 1244-1252.

Murakami, T., Chakoumakos, B.C., Ewing, R.C., Lumpkin, G.R. and Weber, W.J., 1991, Alpha-decay event damage in zircon. *American Mineralogist*, 76: 1510-1532.

Nasdala, L., Irmer, G. and Wolf, D., 1995, The degree of metamictization in zircons: a Raman spectroscopic study. *European Journal of Mineralogy*, 7(3): 471-478.

Nasdala, L., Wenzel, M., Vavra, G., Irmer, G., Wenzel, T. and Kober, B., 2001, Metamictisation of natural zircon: accumulation versus thermal annealing of radioactivity-induced damage. *Contributions to Mineralogy and Petrology*, 141(2): 125-144.

Nasdala, L., Irmer, G. and Jonckheere, R., 2002a, Radiation damage ages: Practical concept or impractical vision?-Reply to two comments on "Metamictisation of natural zircon: Accumulation versus thermal annealing of radioactivity-induced damage", and further discussion. *Contributions to Mineralogy and Petrology*, 143(6): 758-766.

Nasdala, L., Lengauer, C.L., Hanchar, J.M., Kronz, A., Wirth, R., Blanc, P., Kennedy, A.K. and Seydoux-Guillaume, A.-M., 2002b, Annealing radiation damage and the recovery of cathodoluminescence. *Chemical Geology*, 191(1): 121-140.

Nasdala, L., Reiners, P.W., Garver, J.I., Kennedy, A.K., Stern, R.A., Balan, E. and Wirth, R., 2004, Incomplete retention of radiation damage in zircon from Sri Lanka. *American Mineralogist*, 89(1): 219-231.

Oliver, W.C. and McCallum, J.C., 1994, Hardness and elastic modulus of zircon as a function of heavy-particle irradiation dose: II. Pb-ion implantation damage. *Radiation Effects and Defects in Solids*, 132: 131-141.

Özkan, H., 1976, Effect of nuclear radiation on the elastic moduli of zircon. *Journal of Applied Physics*, 47(11): 4772-4779.

Paces, J.B. and Miller, J.D., 1993, Precise U-Pb ages of Duluth Complex and related mafic intrusions, northeastern Minnesota: Geochronological insights to physical, petrogenetic, paleomagnetic, and tectonomagmatic processes associated with the 1.1 Ga Midcontinent Rift System. *Journal of Geophysical Research*, 98(B8): 13997-14013.

Palenik, C.S., Nasdala, L. and Ewing, R.C., 2003, Radiation damage in zircon. *American Mineralogist*, 88(5-6): 770-781.

Paton, C., Woodhead, J., Hellstrom, J., Hergt, J., Greig, A. and Maas, R., 2010, Improved laser ablation U-Pb zircon geochronology through robust downhole fractionation correction. *Geochemistry Geophysics Geosystems*, 11: 1-36.

Paton, C., Hellstrom, J., Paul, B., Woodhead, J. and Hergt, J., 2011, Iolite: Freeware for the visualisation and processing of mass spectrometric data. *Journal of Analytical Atomic Spectrometry*, 26(12): 2508.

Pedersen, R., Dunning, G. and Robins, B., 1989, U-Pb ages of nepheline syenite permatites from the Seiland Magmatic Province, N. Norway. In: Gayer, R. (ed.), The Caledonide Geology of Scandinavia. Graham and Trotman, London, pp. 3-8.

Reddy, S., Timms, N. and Eglington, B., 2008, Electron backscatter diffraction analysis of zircon: A systematic assessment of match unit characteristics and pattern indexing optimization. *American Mineralogist*, 93: 187-197.

Reddy, S., Johnson, T.E., Fischer, S., Rickard, W. and Taylor, R., 2015, Precambrian reidite discovered in shocked zircon from the Stac Fada impactite, Scotland. *Geology*, 43(10): 899-902.

Salje, E.K.H., 2006, Elastic softening of zircon by radiation damage. *Applied physics letters*, 89: 131902.

Schaltegger, U., Schmitt, A.K. and Horstwood, M.S.A., 2015, U-Th-Pb zircon geochronology by ID-TIMS, SIMS, and laser ablation ICP-MS: recipes, interpretations, and opportunities. *Chemical Geology*, 402: 89-110.

Schmitz, M.D., Bowring, S.A. and Ireland, T.R., 2003, Evaluation of Duluth Complex anorthositic series (AS3) zircon as a U-Pb geochronological standard: New high-precision isotope dilution thermal ionization mass spectrometry results. *Geochimica et Cosmochimica Acta*, 67(19): 3665-3672.

Schoene, B., Crowley, J.L., Condon, D.J., Schmitz, M.D. and Bowring, S.A., 2006, Reassessing the uranium decay constants for geochronology using ID-TIMS U–Pb data. *Geochimica et Cosmochimica Acta*, 70: 426-445.

Schoene, B., 2014, U–Th–Pb Geochronology. In: Holland, H. and Turekian, K. (eds.), Treatise on Geochemistry (Second Edition). Elsevier, Oxford.

Sláma, J., Košler, J., Condon, D.J., Crowley, J.L., Gerdes, A., Hanchar, J.M., Horstwood, M.S.A., Morris, G.A., Nasdala, L., Norberg, N., Schaltegger, U., Schoene, B., Tubrett, M.N. and Whitehouse, M.J., 2008, Plešovice zircon — A new natural reference material for U–Pb and Hf isotopic microanalysis. *Chemical Geology*, 249(1-2): 1-35.

Solari, L.A., Ortega-Obregón, C. and Bernal, J.P., 2015, U–Pb zircon geochronology by LAICPMS combined with thermal annealing: Achievements in precision and accuracy on dating standard and unknown samples. *Chemical Geology*, 414: 109-123.

Steely, A., Hourigan, J. and Juel, E., 2014, Discrete multi-pulse laser ablation depth profiling with a single-collector ICP-MS: Sub-micron U–Pb geochronology of zircon and the effect of radiation damage on depth-dependent fractionation. *Chemical Geology*, 372: 92-108.

Taylor, R., Clark, C. and Reddy, S., 2012, The effect of grain orientation on secondary ion mass spectrometry (SIMS) analysis of rutile. *Chemical Geology*, 300-301: 81-87.

van Westrenen, W., Frank, M.R., Hanchar, J.M., Fei, Y., Finch, R. and Zha, C.-S., 2004, In situ determination of the compressibility of synthetic pure zircon (ZrSiO4) and the onset of the zircon-reidite phase transition. *American Mineralogist*, 89: 197-203.

von Allmen, M. and Blatter, A., 1995, Laser-beam interactions with materials. Physical principles and applications. *Springer Series in Materials Science*, vol. 2, Springer-Verlag Berlin Heidelberg, 196 p.

Weis, P., Beck, H.P. and Günther, D., 2005, Characterizing ablation and aerosol generation during elemental fractionation on absorption modified lithium tetraborate glasses using LA-ICP-MS. *Analytical and Bioanalytical Chemistry*, 381(1): 212-224.

Wiedenbeck, M., Allé, P., Corfu, F., Griffin, W.L., Meier, M., Oberli, F., Quadt, A.V., Roddick, J.C. and Spiegel, W., 1995, Three natural zircon standards for U-Th-Pb, Lu-Hf, trace element and REE analyses. *Geostandards Newsletter*, 19(1): 1-23.

Wingate, M. and Compston, W., 2000, Crystal orientation effects during ion microprobe U–Pb analysis of baddeleyite. *Chemical Geology*, 168(1–2): 75-97.

Woodhead, J., Hergt, J., Shelley, M., Eggins, S. and Kemp, R., 2004, Zircon Hf-isotope analysis with an excimer laser, depth profiling, ablation of complex geometries, and concomitant age estimation. *Chemical Geology*, 209(1-2): 121-135.

Woodhead, J.A., Rossman, G.R. and Silver, L.T., 1991, The metamictization of zircon: Radiation dose-dependent structural characteristics. *American Mineralogist*, 76: 74-82.

Zhang, M., Salje, E.K.H., Capitani, G.C., Leroux, H., Clark, A.M., Schlüter, J. and Ewing, R.C., 2000a, Annealing of alpha-decay damage in zircon: a Raman spectroscopic study. *Journal of Physics: Condensed Matter*, 12(13): 3131.

Zhang, M., Salje, E.K.H., Farnan, I., Graeme-Barber, A., Daniel, P., Ewing, R., Clark, A. and Leroux, H., 2000b, Metamictization of zircon: Raman spectroscopic study. *Journal of Physics: Condensed Matter*, 12(8): 1915.